Backbone Dynamics of a Free and a Phosphopeptide-Complexed Src Homology 2 Domain Studied by ^{15}N NMR Relaxation†

Neil A. Farrow,*,‡ Ranjith Muhandiram,‡ Alex U. Singer,§ Steven M. Pascal,‡ Cyril M. Kay,∥ Gerry Gish,⊥ Steven E. Shoelson,# Tony Pawson,⊥ Julie D. Forman-Kay,§,▽ and Lewis E. Kay*,‡

Protein Engineering Network Centres of Excellence and Departments of Medical Genetics, Biochemistry, and Chemistry, University of Toronto, Toronto, Ontario M5S 1A8, Canada, Biochemistry Research Division, Hospital for Sick Children, 555 University Avenue, Toronto, Ontario M5G 1X8, Canada, Medical Research Council Group in Protein Structure and Function, Department of Biochemistry, University of Alberta, Edmonton, Alberta T6G 2H7, Canada, Joslin Diabetes Center and Department of Medicine, Brigham and Women's Hospital, Harvard Medical School, Boston, Massachusetts 02215, and Division of Molecular and Developmental Biology, Samuel Lunefeld Research Institute, Mount Sinai Hospital, 600 University Avenue, Toronto, Ontario M5G 1X5, Canada

Received December 22, 1993; Revised Manuscript Received March 10, 1994®

ABSTRACT: The backbone dynamics of the C-terminal SH2 domain of phospholipase Cγ1 have been investigated. Two forms of the domain were studied, one in complex with a high-affinity binding peptide derived from the platelet-derived growth factor receptor and the other in the absence of this peptide. 2-D ^{1}H–^{15}N NMR methods, employing pulsed field gradients, were used to determine steady-state ^{1}H–^{15}N NOE values and T_1 and T_2 ^{15}N relaxation times. Backbone dynamics were characterized by the overall correlation time (τ_m), order parameters (S^2), effective correlation times for internal motions (τ_e), and, if required, terms to account for motions on a microsecond-to-millisecond-time scale. An extended two-time-scale formalism was used for residues having relaxation data that could not be fit adequately using a single-time-scale formalism. The overall correlation times of the uncomplexed and complexed forms of SH2 were found to be 9.2 and 6.5 ns, respectively, suggesting that the uncomplexed form is in a monomer–dimer equilibrium. This was subsequently confirmed by hydrodynamic measurements. Analysis of order parameters reveals that residues in the so-called phosphotyrosine-binding loop exhibited higher than average disorder in both forms of SH2. Although localized differences in order parameters were observed between the uncomplexed and complexed forms of SH2, overall, higher order parameters were not found in the peptide-bound form, indicating that on average, picosecond-time-scale disorder is not reduced upon binding peptide. The relaxation data of the SH2–phosphopeptide complex were fit with fewer exchange terms than the uncomplexed form. This may reflect the monomer–dimer equilibrium that exists in the uncomplexed form or may indicate that the complexed form has lower conformational flexibility on a microsecond-to-millisecond-time scale.

Many cellular signal recognition pathways rely on the phosphorylation of tyrosine residues by protein tyrosine kinases and the subsequent recognition and binding of these phosphorylated residues by proteins containing Src homology 2 (SH2) domains. These specific recognition domains are found in many proteins involved in signal transduction [for review, see Pawson and Schlessinger (1993)]. SH2 domains contain approximately 100 residues, and structures of the domain in a number of proteins have been solved. The structure of the Src SH2 domain was determined by X-ray crystallography in complex with both low- and high-affinity binding phosphotyrosine peptides (Waksman et al., 1992, 1993). The structure of the Lck SH2 domain in complex with a high-affinity binding peptide as determined by X-ray crystallography has also been published recently (Eck et al., 1993). Nuclear magnetic resonance solution structures have been determined for the isolated SH2 domains of the Abl tyrosine kinase (Overduin et al., 1992) and the p85 subunit of phosphoinositol-3′-OH kinase (Booker et al., 1992). These structures reveal that the SH2 domain consists of a central β-sheet core, containing a three-stranded antiparallel β-sheet and a smaller, contiguous but distinct, antiparallel β-sheet. Two α-helices are located on opposite sides of the β-sheet core. The structures of SH2 in complex with phosphotyrosine peptides demonstrate that residues on one side of the large β-sheet and in the N-terminal α-helix are involved in binding the phosphotyrosine residue. The peptide spans the edge of the large β-sheet, with residues C-terminal to the phosphotyrosine interacting with residues in the smaller β-sheet and the second α-helix.

While a common structural motif has been identified for the SH2 domain, the mechanism of sequence-specific binding remains less clear. It is apparent that the specificity arises from the ability of the SH2 domains to recognize the phosphotyrosine in the context of the residues that immediately surround it. From studies of SH2 binding to peptide libraries, sequences which preferentially bind to different SH2 domains have been determined. In particular, it has been shown that the three residues C-terminal to the phosphotyrosine play a critical role in conferring specificity on a given SH2 domain (Songyang et al., 1993).

† This work was supported through grants from the Natural Sciences and Engineering Research Council of Canada (L.E.K.) and the National Cancer Institute of Canada (J.D.F. and L.E.K.) with funds from the Canadian Cancer Society.

* Authors to whom correspondence should be addressed.
‡ Protein Engineering Network Centres of Excellence and Departments of Medical Genetics, Biochemistry, and Chemistry, University of Toronto.
§ Hospital for Sick Children.
∥ University of Alberta.
⊥ Mount Sinai Hospital.
Harvard Medical School.
▽ Department of Biochemistry, University of Toronto.

® Abstract published in *Advance ACS Abstracts*, April 15, 1994.

0006-2960/94/0433-5984$04.50/0

```
                        βA    αA              βB          βC
                        |     |               |           |
src                     WYFGKITRRESERLLLNPENPRGTFLVRESETTKGAYCLSVSDFDNAK
lck                     WFFKNLSRKDAERQLLAPGNTHGSFLIRESESTAGSFSLSVRDFDQNQ
PLCγ1C      GSPGIHESKEWYHASLTRAQAEHMLMRVPRD GAFLVRKRNEPN SYAISFRA E
                        |         |         |         |         |
                        10        20        30        40        50

                      βD     βD'    βE     βF  αB                  βG
                      |      |      |      |   |                   |
src         GLNVKHYKIRKLDSG GFYITSRTQFSSLQQLVAYYSKHADGLCHRLTNVC
lck         GEVVKHYKIRNLDNG GFYISPRITFPGLHDLVRHYTNASDGLCTRLSRPC
PLCγ1C      G KIKHCRVQQE  GQTVMLGN SEFDSLVDLISYYEKHPLYRKMKLRYPINEENSS
                      |         |         |         |         |
                      60        70        80        90        100
```

FIGURE 1: Primary sequence alignment of the SH2 domains of Src, Lck, and PLCγ1C. Elements of conserved secondary structure are indicated by underlining. The boundaries of secondary structural elements in the PLCγ1C SH2 domain are based on preliminary solution structure data (Pascal et al., 1994). The nomenclature proposed by Harrison and co-workers (Eck et al., 1993) is used to refer to the conserved secondary structural elements and is indicated above the first residue of each element. The residue numbers underneath the PLCγ1C sequence are used in the text to refer to individual amino acids of the construct of the PLCγ1C domain used in this study.

In order to better understand the biological nature of SH2 binding, we are studying the C-terminal SH2 domain of phospholipase Cγ1 (PLCγ1C SH2) in complex with a 12-residue phosphopeptide, DNDpYIIPLPDPK (pY1021). This sequence corresponds to a high-affinity phosphotyrosine-binding site from the Tyr 1021 position of the platelet-derived growth factor (PDGF) receptor and is one of eight autophosphorylation sites in the cytoplasmic portion of the receptor (Anderson et al., 1990). Mutation of Tyr 1021 to Phe leads to disruption of a biologically significant interaction of phospholipase Cγ1 with the PDGF receptor (Valius et al., 1993). The dissociation constant for the PLCγ1C SH2–pY1021 peptide complex is approximately $1–5 \times 10^{-7}$ M, as estimated by competition assays (Piccione et al., 1993) and calorimetry (Shoelson, unpublished results). These estimates are consistent with determinations of the concentration of pY1021 peptide required for 50% inhibition of binding of intact PLCγ1 to the C-terminal tail of the PDGF receptor (Larose et al., 1993). Furthermore, protein–peptide NMR titration studies indicate that the binding is specific and that the complex exists in slow exchange on the NMR time scale. Figure 1 shows a primary sequence alignment of the Lck, Src, and PLCγ1C SH2 domains. The nomenclature used in referring to specific residues in secondary structural elements is the same as that used in the study of Lck (Eck et al., 1993). A preliminary 3D structure for the phospholipase Cγ1 C-terminal SH2 domain has been determined and is shown in Figure 2, which illustrates the secondary structural elements of the domain. The structure is broadly similar to those of other SH2 domains; detailed analysis of the PLCγ1C SH2 structure will be published elsewhere (Pascal et al., 1994).

In this paper, the results of ^{15}N NMR relaxation studies of the free PLCγ1C SH2 domain and of the SH2 domain in complex with the pY1021 peptide are described. These studies permit characterization of the backbone dynamics of the SH2 domain. Solution structures of SH2 domains have suggested that there are a number of mobile loops in the structures and that the mobility of these loops may play an important role in peptide recognition and specificity of peptide binding. This assertion is supported by loop-associated, high B-factors in the published Src SH2 structure of the protein–peptide complex. Use of ^{15}N NMR relaxation studies of the SH2 domain alone, and in complex with a high-affinity binding peptide, allows examination of the differential dynamics of the two forms. Analysis of the changes in the dynamic characteristics of specific residues in the protein, in addition to being indicative of their involvement in peptide binding, may provide insight into the nature of protein–protein recognition.

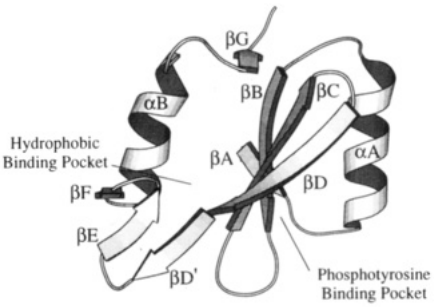

FIGURE 2: Schematic diagram of the 3D solution structure of the SH2 domain of phospholipase Cγ1C (Pascal et al., 1994). Secondary structural features are indicated using the same nomenclature as in Figure 1. The high-affinity binding peptide pY1021 binds across the edge of the βD strand of the SH2 domain, interacting with the phosphotyrosine- and hydrophobic binding pockets indicated in the diagram. The figure was generated using the program Molscript (Kraulis, 1991).

MATERIALS AND METHODS

Sample Preparation. PLCγ1C SH2 was subcloned into a PET11d expression vector under the control of the T7 promoter in *Escherichia coli* BL21 cells. The bacteria were grown at 37 °C in M9 minimal media, supplemented with 10 mg/L biotin, 10 mg/L thiamine, 0.3% glucose, and 0.1% $^{15}NH_4Cl$. When the OD reached 0.7, IPTG was added to 250 mg/L, and expression was induced for 4 h at 30 °C. Cells were then centrifuged for 20 min at 5000 rpm. Pellets were resuspended in 20 mM sodium phosphate, pH 7, 150 mM NaCl, 1 mM benzamidine, 1 mM EDTA, 5 mM DTT, and 1% Triton X-100, sonicated (pulsed) for 1 min five times, and centrifuged for 10 min at 8000 rpm. The residual pellets were resuspended and resonicated two additional times. Pooled supernatents were passed over a phosphocellulose column with a 0.15–1.5 M NaCl gradient. The pooled fractions were further purified over a phenyl sepharose column using a 1.5–0.15 M NaCl gradient. Some of the protein preparations required a final purification over a MonoS column with a 0.0–1.0 M NaCl

gradient. Care was taken to prevent oxidation of the single cysteine in the protein by reduction of the pure protein in excess DTT, dialysis in argon-purged buffers to lower the DTT concentration to 0.05 mM, and sealing the sample in an argon-blanketed NMR tube. Protein concentrations were determined using an extinction coefficient of 0.87 OD per mg/mL protein, calculated from sedimentation equilibrium centrifugation measurements. NMR samples of 500 μL contained 1.0–1.5 mM ^{15}N-labeled PLCγ1C SH2 in 100 mM sodium phosphate, pH 6.4, 90% H_2O/10% D_2O. For preparation of the phosphopeptide complex, lyophilized synthetic HPLC-purified pY1021 was added to the SH2 in solution to yield a slight excess of peptide relative to the PLCγ1C SH2 in the final samples.

Sedimentation Equilibrium and Laser Light Scattering. Sedimentation equilibrium experiments were performed at 20 °C by using conventional low-speed techniques and a Beckman Model E analytical ultracentrifuge equipped with electronic speed control and Rayleigh interference optics. Determinations of molecular weights were made using the conventional sedimentation equilibrium technique as described by Chervenka (1969); 100 μL of each sample which had been dialyzed against buffer solution for 48 h was loaded into 12-mm double-sector, charcoal-filled Epon cells equipped with Sapphire windows. The sedimentation equilibrium runs were performed for approximately 48 h before equilibrium photographs were taken. Measurements of photographic plates were performed on a Nikon Model 6C microcomparator. Molecular weight calculations were carried out using a computer program written in the APL language. An assumed value of 0.73 was used for the partial specific volume of both the uncomplexed and complexed forms of SH2. Data of the form $\ln(y)$ vs r^2, where y is the optical density and r is the distance traveled in the centrifuged cell, were fit to a second-degree polynomial equation using least-squares techniques and a point-averaged molecular weight calculated from the slope of this equation.

Molecular weight determinations using light-scattering techniques were performed on a Dawn F multiangle laser light-scattering photometer, manufactured by Wyatt Technology Corporation, according to methodology described in the Dawn F instrument manual and by Wyatt (1993). Relatively low-concentration molecular weight determinations were made by injecting samples onto a gel filtration column attached to the instrument. Concentrations for the eluting peaks from the column were measured on the basis of the differential refractive index increment of the sample (dn/dc). Apparent weight-averaged molecular weights were calculated for each peak using Debye plots by extrapolation to 0° angle. Determinations of molecular weights at higher sample concentrations were performed with the gel filtration column removed from the system. In this case, a series of concentrations were injected directly into the apparatus using a manual injector. A value of 0.185 was used for dn/dc.

NMR Spectroscopy. The pulse sequences used to record ^{15}N T_1 and T_2 values are shown in Figure 3a,b, respectively, and the scheme for measurement of the steady-state ^{1}H–^{15}N NOE is indicated in Figure 3c. All three pulse sequences are similar to those reported previously in the literature. However, in the present case, we have employed pulsed field gradients in order to minimize the artifact content of the spectra, suppress the intense solvent resonance, and select for the coherence transfer pathway whereby magnetization passes from ^{15}N to ^{1}H for observation. Bax and Pochapsky (1992) have described in detail the use of gradients to eliminate artifacts in spectra. Following their lead, we have inserted equal gradient pulses on opposite sides of simultaneous ^{1}H/^{15}N 180° pulses in order to ensure that only transverse magnetization present before and after the application of the pulse pair is refocused. In addition, gradients are inserted during intervals when the magnetization is of the form I_zN_z, where I_z and N_z denote the z components of NH and ^{15}N magnetization, respectively. In addition to eliminating artifacts due to pulse imperfections, insertion of gradients during these periods in the sequences aids in the suppression of the water resonance. In order to ensure that magnetization originates on ^{1}H and not ^{15}N in the case of the T_1 and T_2 measurements, the T_1 and T_2 sequences begin with a 90° ^{15}N pulse followed by the application of a gradient pulse to dephase any magnetization in the transverse plane. The heavily shaded gradients in Figure 3 are used for coherence transfer selection. As discussed previously (Kay et al., 1992a; Muhandiram & Kay, 1993), the use of pulsed field gradients to select for coherence transfer pathways in combination with the enhanced sensitivity method developed by Rance and co-workers (Cavanagh et al., 1991; Palmer et al., 1991) generates spectra that are free of artifacts, have excellent water suppression levels, and increased sensitivity by as much as a factor of $\sqrt{2}$ relative to unenhanced, nongradient spectra. A recent comparison of spectra recorded on a number of different proteins ranging in molecular weight from approximately 10 to 20 kDa showed that when using the enhancement approach of Rance and co-workers, the use of gradients for pathway selection does not decrease the sensitivity of spectra (Muhandiram & Kay, 1993).

^{1}H–^{15}N steady-state NOE values are obtained by recording spectra with (NOE experiment) and without (NONOE experiment) the use of ^{1}H saturation applied before the start of the experiment. The level of water suppression in spectra recorded without ^{1}H saturation is often significantly worse than that in the ^{1}H saturation case and can lead to difficulties in obtaining accurate values for peak intensities. Moreover, any saturation of protons prior to the start of the NONOE experiment gives rise to a small truncated NOE effect. Therefore, suppression of the strong H_2O resonance is achieved via the use of gradients to select for the ^{15}N → ^{1}H coherence transfer pathway and the application of a ^{1}H 90° pulse followed by a gradient pulse immediately prior to the start of the experiment to eliminate ^{1}H magnetization. Elimination of all ^{1}H magnetization (including solvent) in this way can be achieved in 2–3 ms, which is sufficiently short that ^{1}H–^{15}N cross-relaxation may safely be neglected during this interval.

Similar pulse schemes which have the additional benefit of reducing deleterious effects which arise from the saturation of water are described in the Appendix.

^{15}N T_1 and T_2 and ^{1}H–^{15}N NOE spectra were recorded at 30 °C on a Varian Unity 500-MHz spectrometer equipped with a triple-resonance, pulsed field gradient probe with an actively shielded z gradient and a gradient amplifier unit. ^{15}N T_1 values were measured from the spectra recorded with eight different durations of the delay T: T = 5, 65, 145, 246, 366, 527, 757, and 1148 ms. T_1 spectra were recorded with magnetization relaxing as $\exp(-T/T_1)$ and in such a way that the delay between scans affected only the sensitivity and not the extracted T_1 values (Sklenar et al., 1987). T_2 values were determined from spectra recorded with delays T = 8.4, 25.1, 41.8, 58.6, 75.3, 108.8, and 142.3 ms. To permit the estimation of noise levels, duplicate spectra were recorded for T = 246

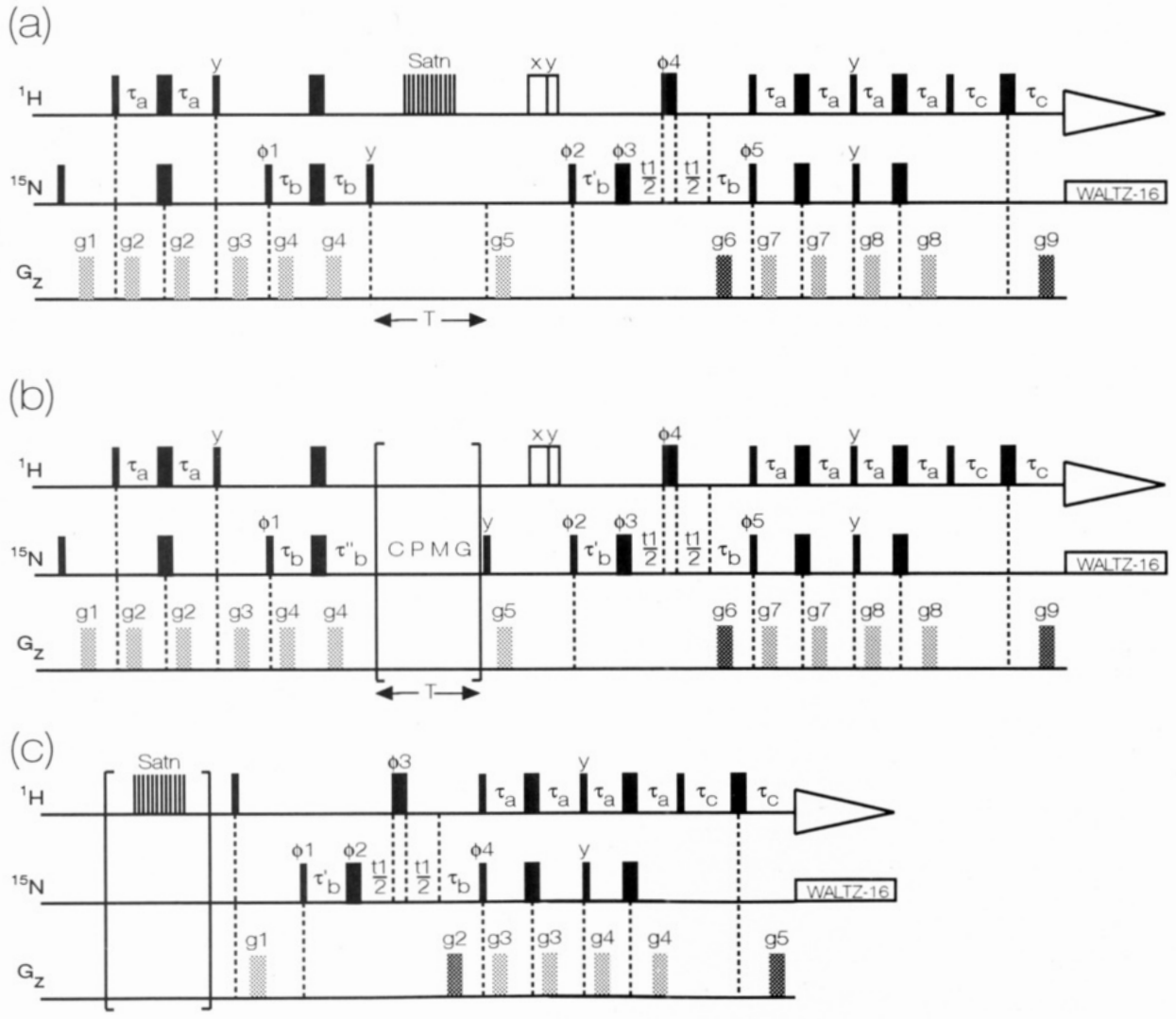

FIGURE 3: Enhanced sensitivity pulse sequences employing pulsed field gradients for the measurement of (a) ^{15}N T_1, (b) ^{15}N T_2, and (c) ^{1}H–^{15}N NOE values. In all sequences, narrow and wide pulses indicate 90° and 180° pulses, respectively, darker gradient pulses indicate those used for coherence transfer selection, and, unless indicated otherwise, all pulses are applied along the x-axis. The value of τ_a was set to 2.25 ms ($<1/(4J_{NH})$), τ_b was set to 2.75 ms ($1/(4J_{NH})$), and τ_c was set to 0.5 ms in all experiments. The delay τ'_b is set according to the relation: $\tau'_b = \tau_b + 2$pw, where pw is the width of the ^{1}H 90° pulse. The delay τ''_b is set as: $\tau''_b = \tau_b + (2/\pi)$pwn, where pwn is the 90° ^{15}N pulse width. WALTZ-16 decoupling (Shaka et al., 1983) of ^{15}N during acquisition was achieved using a 1-kHz field. Phase cycling used for the T_1 and T_2 experiments is $\phi1 = x, -x$; $\phi2 = y$; $\phi3 = 4(x), 4(y), 4(-x), 4(-y)$; $\phi4 = 2(x), 2(-x)$; $\phi5 = x$; and receiver is $x, -x, x, -x, -x, x, -x, x$. In sequences a and b, for each t_1 value, two FIDs are recorded and stored separately with the phase of $\phi5$ incremented by 180° (from x to $-x$) and the amplitude of the gradient pulse g6 is inverted for the second FID. Signals recorded for a given t_1 value and stored in separate memory locations are manipulated, postacquisition, in a manner described previously (Kay et al., 1992a) to generate pure absorption data which are subsequently processed using the method of STATES (States et al., 1982). For each increment of t_1, the phases of $\phi2$ and the receiver are incremented by 180°. In order to obtain slightly better water suppression, 10-kHz x,y ^{1}H purge pulses (Messerlie et al., 1989) of duration 8.0 and 4.9 ms, respectively, can be applied at the conclusion of the T period. In the case of the T_2 experiment (Figure 3b), ^{15}N magnetization is returned to the z-axis prior to the purge pulses. The CPMG sequence (Carr & Purcell, 1954; Meiboom & Gill, 1958) used includes ^{1}H 180° pulses to eliminate the effects of cross-correlation between ^{1}H–^{15}N dipolar coupling and chemical shift anisotropy relaxation mechanisms as described by Kay et al. (1992b) and Palmer et al. (1992). A delay of 0.9 ms is inserted between successive applications of ^{15}N 180° pulses with ^{1}H 180° pulses applied every 4 ms in the CPMG pulse train. In order to reduce heating during the CPMG portion of the T_2 pulse sequence, a field of 3.4 kHz was employed for all ^{15}N pulses, while a field of 5.3 kHz was used for ^{15}N pulses in sequences a and c. The phase cycling for the NOE experiment was $\phi1 = y$; $\phi2 = 2(x), 2(y), 2(-x), 2(-y)$; $\phi3 = x, -x$; $\phi4 = x$; and receiver was $x, x, -x, -x$. For each increment of t_1, two FIDS are collected with the phase of ϕ_4 and the amplitude of the gradient pulse g5 inverted in the second FID. For each increment of t_1, the phases of ϕ_1 and the receiver are incremented by 180°. ^{1}H saturation is achieved by the application of 120° pulses (Markley et al., 1971) spaced at 5-ms intervals for 3 s prior to the first ^{15}N pulse. An overall delay between scans of 5 s was employed in both the NOE and NONOE experiments. T_1 and T_2 sequence gradient durations and levels are as follows: g1 = 1 ms, 5 Gcm^{-1}; g2 = 0.5 ms, 4 Gcm^{-1}; g3 = 2 ms, 10 Gcm^{-1}; g4 = 0.5 ms, 8 Gcm^{-1}; g5 = 1 ms, 10 Gcm^{-1}; g6 = 1.25 ms, 30 Gcm^{-1}; g7 = 0.5 ms, 4 Gcm^{-1}; g8 = 0.5 ms, 4 Gcm^{-1}; and g9 = 0.125 ms, 27.8 Gcm^{-1}. Gradient levels and durations in the NOE experiment: g1 = 3 ms, –20 Gcm^{-1}; g2 = 1.25 ms, 30 Gcm^{-1}; g3 = 0.5 ms, 4 Gcm^{-1}; g4 = 0.5 ms, 4 Gcm^{-1}; and g5 = 0.125 ms, 27.8 Gcm^{-1}.

ms (T_1 spectra) and T = 8.4 and 58.6 ms (T_2 spectra). In order to eliminate the effects of cross-correlation between ^{1}H–^{15}N dipolar and ^{15}N CSA relaxation mechanisms, ^{1}H 180° pulses were inserted during the T relaxation times as described by Boyd et al. (1990), Palmer et al. (1992), and Kay et al. (1992b). NOE values were determined from spectra recorded in the presence and absence of a proton presaturation period of 3 s. ^{1}H saturation was achieved with the use of 120° ^{1}H pulses applied every 5 ms (Markley et al., 1971). In the case of the NONOE spectra, a net relaxation delay of 5 s was employed, while a relaxation delay of 2 s prior to a 3-s proton presaturation period was employed for the NOE spectra. Relaxation delays of 1 s were employed in the measurement of ^{15}N T_1 and T_2 values.

Data Processing and Analysis. All spectra were recorded as 160 × 512 complex matrices with 32 scans per t_1 point. Spectral widths of 1650 and 8000 Hz were employed in F_1 and F_2, respectively. In order to generate pure absorptive 2D line shapes, N- and P-type signals recorded for a given t_1 value were stored in separate memory locations, where they could be added and subtracted, and a 90° zero-order phase correction was applied to every other FID. Because of the excellent H_2O suppression afforded by the use of gradients, it was not necessary to remove residual water through the use of time domain deconvolution routines (Marion et al., 1989). Data processing was performed using a combination of software from New Methods Research (Syracuse, NY) and software written in-house. All spectra were processed identically with Lorentzian–Gaussian apodization functions applied in both dimensions.

The intensities of the peaks in the 2-D spectra were described by peak heights as determined by the peak-picking package in the commercial software (New Methods Research). A comparative study of decays characterized by both peak heights and peak volumes was performed for the T_1 data of uncomplexed SH2 and was found to yield essentially the same results (data not shown).

T_1 and T_2 values were determined by fitting the measured peak heights to a two-parameter function of the form

$$I(t) = I_0 \exp(-t/T_{1,2}) \quad (1)$$

where $I(t)$ is the intensity after a delay of time t and I_0 is the intensity at time $t = 0$. A conjugate gradient minimization (Press et al., 1986) was performed to determine the optimum value of the I_0 and $T_{1,2}$ parameters by minimizing the χ^2 goodness of fit parameter

$$\chi^2 = \sum (I_c(t) - I_e(t))^2/\sigma_I^2 \quad (2)$$

where $I_c(t)$ are the intensities calculated from the fitting parameters, $I_e(t)$ are the experimental intensities, σ_I is the standard deviation of the experimental intensity measurements, and summation is performed over the number of time points recorded in each experiment. The goodness of fit of the data to the single-exponential decay function given in eq 1 can be assessed by comparing the calculated χ^2 value to tabulated values of χ^2 at 95% confidence levels (Palmer et al., 1991). Monte Carlo simulations were performed to estimate the uncertainty of the relaxation parameters (Kamath & Shriver, 1989; Palmer et al., 1991; Press et al., 1986).

The steady-state NOE values were determined from the ratios of the average intensities of the peaks with and without proton saturation. The standard deviation of the NOE value, σ_{NOE}, was determined on the basis of measured background noise levels using the following relationship

$$\sigma_{NOE}/NOE = ((\sigma_{Isat}/I_{sat})^2 + (\sigma_{Iunsat}/I_{unsat})^2)^{1/2} \quad (3)$$

where I_{sat} and I_{unsat} represent the measured intensities of a resonance in the presence and absence of proton saturation, respectively. The standard deviations of these values, calculated from the root-mean-square noise of background regions, are represented by σ_{Isat} and σ_{Iunsat}.

The root-mean-square (rms) value of the background noise regions was used to estimate the standard deviation of the measured intensities. The duplicate spectra that were collected were used to assess the validity of this estimate. The distribution of the difference in intensities of identical peaks in duplicate spectra should have a standard deviation $\sqrt{2}$ times greater than the standard deviation of the individual peaks. This analysis was performed for the SH2 data, and the two measures were found to agree (average discrepancy of 7%). On this basis, it was concluded that the rms value of the noise could be used to estimate the standard deviations of the measured intensities.

The T_1 and T_2 relaxation times and the NOE enhancement of an amide ^{15}N nucleus are dominated by the dipolar interaction of the ^{15}N nucleus with its attached proton and by chemical shift anisotropy as described by (Abragam, 1961)

$$1/T_1 = d^2[J(\omega_H - \omega_N) + 3J(\omega_N) + 6J(\omega_H + \omega_N)] + c^2J(\omega_N) \quad (4)$$

$$1/T_2 = 0.5d^2[4J(0) + J(\omega_H - \omega_N) + 3J(\omega_N) + 6J(\omega_H) + 6J(\omega_H + \omega_N)] + (^1/_6)c^2[3J(\omega_N) + 4J(0)] \quad (5)$$

$$NOE = 1 + (\gamma_H/\gamma_N)d^2[6J(\omega_H + \omega_N) - J(\omega_H - \omega_N)]T_1 \quad (6)$$

The constants d^2 and c^2 are defined as

$$d^2 = 0.1\gamma_H^2\gamma_N^2h^2/(4\pi^2)(1/r^3_{NH})^2 \quad (7)$$

$$c^2 = (^2/_{15})\gamma_N^2H_0^2(\sigma_\parallel - \sigma_\perp)^2 \quad (8)$$

where γ_H and γ_N are the gyromagnetic ratios of the ^1H and ^{15}N nuclei, respectively, ω_H and ω_N are the ^1H and ^{15}N Larmor frequencies, r_{NH} is the internuclear ^1H–^{15}N distance (1.02 Å), H_0 is the magnetic field strength, and the parallel and perpendicular components of the assumed axially symmetrical ^{15}N chemical shift tensor are represented by $\sigma_\parallel$ and $\sigma_\perp$, respectively. The assumption of an axially symmetric chemical shift tensor has been shown to be valid for peptide bonds with $(\sigma_\parallel - \sigma_\perp) = -160$ ppm (Hiyama et al., 1988).

The spectral density function can be represented using a model-free formalism (Lipari & Szabo, 1982a,b) which employs a minimum number of parameters to describe the overall tumbling motion of a macromolecule and the internal motions of the ^1H–^{15}N bond vector, in the following expression:

$$J(\omega) = S^2\tau_m/(1 + \omega^2\tau_m^2) + (1 - S^2)\tau/(1 + \omega^2\tau^2) \quad (9)$$

The order parameter S^2 describes the degree of spatial restriction of the internal motion of the ^1H–^{15}N bond vector; τ_m is the correlation time as a result of the tumbling motion of the entire molecule. The effective correlation time resulting from internal motions is described by τ_e, where $1/\tau = 1/\tau_m + 1/\tau_e$. Equation 9 assumes that the overall tumbling is isotropic; the validity of this assumption for the molecule described here will be discussed below.

An extended form of the model-free spectral density function has been developed (Clore et al., 1990a,b) to describe internal motions that take place on two distinct time scales, differing by at least an order of magnitude. Assuming that the term containing the correlation time describing the faster of the two time scales contributes a negligible amount to the relaxation, the modified spectral density function becomes (Clore et al., 1990b)

$$J(\omega) = S^2\tau_m/(1 + \omega^2\tau_m^2) + (S_f^2 - S^2)\tau/(1 + \omega^2\tau^2) \quad (10)$$

where the order parameter S^2 is expressed as the product of two order parameters characterizing the fast and slow internal motions, S_f^2 and S_s^2, respectively. The effective correlation

time for the slow internal motions, τ_s, is included using the relationship $1/\tau = 1/\tau_s + 1/\tau_m$.

An additional term, R_{ex}, is required when modeling observed transverse relaxation rates to account for the contributions from processes other than those from dipole–dipole and chemical shift anisotropy. In many cases, these contributions are the result of conformational exchange averaging. The additional term, R_{ex}, may be included to modify the calculated T_2 value using the following relationship

$$1/T_2 = 1/T_{2(DD)} + 1/T_{2(CSA)} + R_{ex} \quad (11)$$

in which the DD and CSA subscripts indicate the contributions of dipole–dipole and chemical shift anisotropy to transverse relaxation.

In order to determine the most appropriate spectral density function for modeling the relaxation parameters of each residue, the following process of elimination was performed. Relaxation parameters calculated from the spectral density functions were compared to experimental values using a χ^2 function defined as

$$\chi^2 = (T_{1c} - T_{1e})^2/\sigma_{T1}^2 + (T_{2c} - T_{2e})^2/\sigma_{T2}^2 + (NOE_c - NOE_e)^2/\sigma_{NOE}^2 \quad (12)$$

where the subscripts c and e represent calculated and experimentally determined relaxation parameters, respectively, and σ_{T1}, σ_{T2}, and σ_{NOE} are estimates of the standard deviation of the experimentally determined parameters. Nonlinear least-squares optimizations and Monte Carlo error analyses were performed for the variables in each of the following spectral density functions: a function of the form given in eq 9 with τ_e fixed at zero, the same function with τ_e used as a fitting parameter, the functional form described in eq 9 with τ_e fixed at zero but including the term R_{ex} to account for conformational exchange, the functional form in eq 9 including both τ_e and R_{ex} as fitting parameters, and finally the two-time-scale form of the spectral density function given in eq 10.

Selection of the appropriate spectral density function was performed in the following manner. Initially, the spectral density function utilizing two time scales, eq 10, was not considered. The four remaining spectral density functions were considered to be appropriate if they satisfied two conditions. First, all three relaxation parameters must be fit within 95% confidence limits, defined as 1.96 times the experimental standard deviation. Second, each of the fitting parameters in the spectral density functions must exceed its calculated error. If more than one of the spectral density functions satisfied both conditions, then the model with the lowest χ^2 (as defined in eq 12) was selected. Only if none of the single-time-scale spectral density functions were able to satisfy both of the above conditions was the two-time-scale spectral density function considered. If the two-time-scale model satisfied similar constraints on both the fit to the relaxation parameters and the significance of the fitting parameters, then it was selected to model the relaxation data of that particular residue.

In order for the correct spectral density function to be determined, it is necessary to obtain a value for the overall correlation time of the molecule, τ_m. As has been described earlier (Kay et al., 1989; Clore et al., 1990a), the ratio of T_1 and T_2 may be used to estimate τ_m, provided that $\tau_e < 100$ ps, $\tau_m > 1$ ns, and T_2 is not shortened by chemical exchange. In this situation, the ratio of T_1/T_2 is effectively independent of both the order parameter S^2 and the effective correlation time τ_e. Theoretical values of the T_1/T_2 ratio may then be calculated for a given τ_m using the spectral density function in eq 9 with S^2 set to unity and τ_e set to zero and compared to experimental T_1/T_2 ratios to extract the appropriate values of τ_m on a per residue basis.

Residues with a T_1/T_2 ratio one standard deviation greater than the mean were excluded from the initial determination of τ_m on the basis that conformational exchange was probably contributing to a reduction in the T_2 value (Clore et al., 1990a). Residues with a T_1/T_2 ratio one standard deviation smaller than the mean were excluded on the grounds that they may be more correctly modeled using a two-time-scale spectral density function as in eq 10. For each residue, the τ_m giving rise to the best fit between calculated and measured T_1/T_2 ratios was determined. An estimate of the global optimum for τ_m was obtained from the average of the individual values.

Following the determination of the appropriate spectral density function for each residue, the overall correlation time was optimized for all the residues simultaneously. Once the global optimum τ_m value had been determined, the process of fitting the relaxation parameters on a per residue basis was repeated using the selected spectral density function.

RESULTS

Figure 4 shows a region taken from T_1 spectra of the complexed SH2 domain at three different delays, demonstrating the quality of the recorded data. Of the 100 possible correlations involving backbone amide protons, relaxation data were obtained for 82 and 80 residues in the uncomplexed and complexed forms of PLCγ1C SH2, respectively. Resonance overlap was the major cause of difficulties in measuring peak intensities in the T_1, T_2, and NOE spectra, with some problems due to extremely weak resonances caused by rapid amide–solvent exchange and the two N-terminal amide resonances being unassigned.

Measured Relaxation Parameters. Single-exponential two-parameter decay curves were fit to the decay data (see eq 1). For the measurements performed on the uncomplexed form of the SH2 domain, it was found that intensities of the first time point were biased with respect to the rest of the series, with the values consistently falling below those expected for an exponential decay. As a result, these data were excluded in the fitting procedure. For the T_1 and T_2 series of measurements on the uncomplexed SH2 domain, χ^2 values indicated that 69 and 64 residues, respectively, were adequately fit by the two-parameter decay curve. For the peptide-complexed SH2 domain, the model was statistically adequate for 75 T_1 decays and 73 T_2 decays. These levels of sufficiency are similar to those seen by other authors (Stone et al., 1992; Palmer et al., 1991). Palmer noted for his study that there was insufficient data to warrant using a three-parameter decay function and ascribed the poor fitting to underestimation of uncertainty in measured peak heights. Figure 5 illustrates examples of the exponential fit to measured longitudinal and transverse relaxation data for the two forms of SH2.

The values of the relaxation parameters, T_1, T_2, and NOE, are shown in Figure 6 for both the uncomplexed and peptide-complexed states of the SH2 domain. The average value of T_1 in the uncomplexed state is 613 ms, and in the peptide-complexed form, the average value is 510 ms. The average values of T_2 in the uncomplexed and complexed forms are 98 and 130 ms, respectively. It can be seen from Figure 6 that the overall pattern of variations in the T_1 and T_2 values as a function of residue number is similar for the two states.

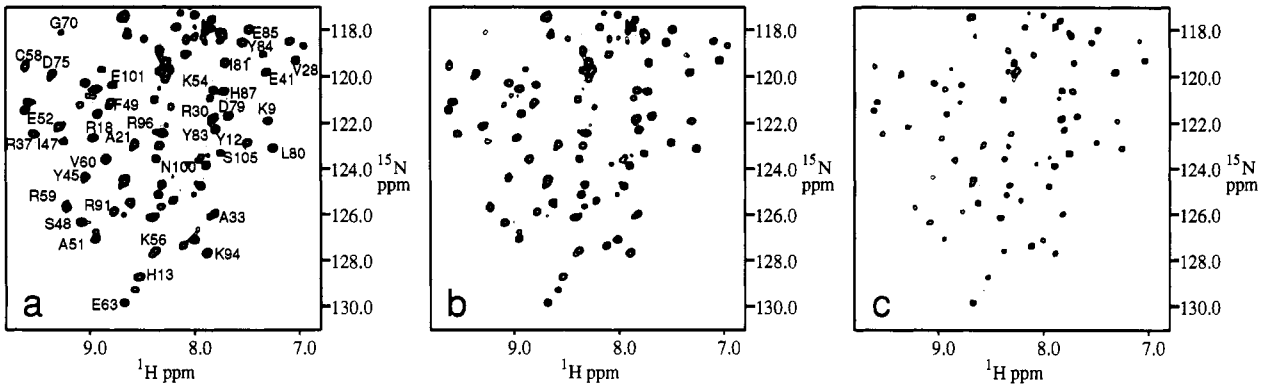

FIGURE 4: Region of the ^{1}H–^{15}N shift correlation spectrum recorded with the pulse sequence used to determine T_1 as shown in Figure 3a and three relaxation delay values (T) of (a) 5, (b) 246, and (c) 757 ms.

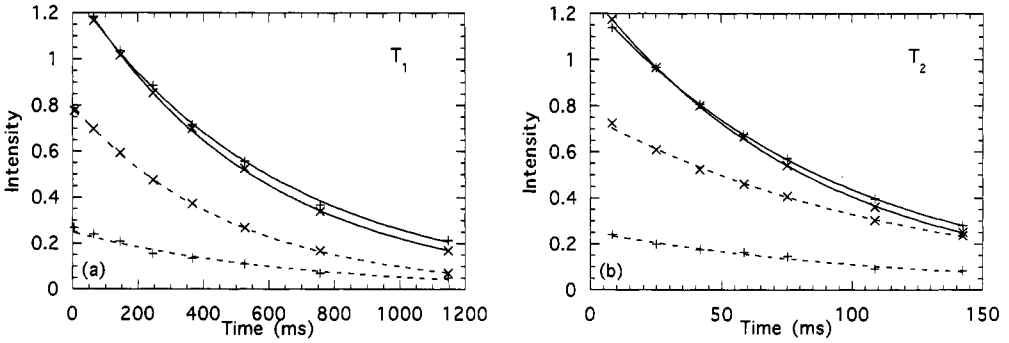

FIGURE 5: Examples of (a) T_1 and (b) T_2 decay curves for Ser 44 (+) and Leu 80 (×) in the uncomplexed (solid lines) and pY1021 peptide-complexed (dashed lines) forms. The curves indicate best fits to single-exponential decays. Error bars, if shown, would be smaller than the size of the characters used to indicate the data points.

There are a number of regions of the protein where the values of T_1 are significantly different from the average value. In the uncomplexed state, residues Glu 41 and Asn 43 have significantly increased T_1 values; in the complexed form, both Asn 40 and Glu 41 have larger values. Residue Arg 30 also has a large T_1 value in both forms of SH2. A number of trends, not necessarily monotonic, over multiple residues are seen in both the uncomplexed and complexed forms of SH2. The T_1 value gradually increases from around residue Arg 50 to a maximum value at residue Thr 66. The T_1 value then decreases toward a minimum value at Ile 81 before increasing again to residue Tyr 90 in the uncomplexed form and to residue Leu 89 in the complexed form. The C-terminal residues Ser 104 and Ser 105 show markedly increased T_1 values in both forms. The average error in the calculated T_1 value was 1.2% in the uncomplexed form and 2.4% in the complexed form.

The T_2 values show similar sequential variations to those described for T_1 above. The T_2 values are again seen to increase to a maximum value at Thr 66; however, in the uncomplexed form, this pattern is less pronounced. The four C-terminal residues, Glu 101, Glu 102, Ser 104, and Ser 105, all exhibit increased transverse relaxation times. Residues Arg 30 and Glu 41 exhibit above average values of T_2 in both forms of SH2. In the uncomplexed form, residue Arg 39 has an above average T_2 value which is not seen in the complexed form. In the complexed form, above average transverse relaxation times are seen for residues Ala 14 and Leu 16 (and interestingly not Ser 15). In both forms, the T_2 value for the most N-terminal residue whose transverse relaxation time could be measured, Ile 5, is seen to be above average. The average Monte Carlo error estimate for the calculated T_2 values is 1.4% for the uncomplexed form and 3.3% in the peptide-complexed form.

The average steady-state NOEs determined from the two separate measurements are plotted in Figure 6. Note that the NOE values do not exceed the theoretical maximum by more than their estimated errors. In the uncomplexed form of the SH2 domain, those residues which have NOE values more than one standard deviation below the mean (calculated excluding the negative NOEs in the C-terminal region) are Ile 5, Arg 30, Arg 39, Glu 41, Thr 66, Glu 101, Glu 102, Ser 104, and Ser 105. A similar analysis of the steady-state NOEs for the complexed form of SH2 shows significantly lower values associated with residues Ile 5, Leu 16, Arg 30, Phe 34, Glu 41, Ala 51, Thr 66, Glu 102, Ser 104, and Ser 105. There is a gradual decrease, more pronounced in the uncomplexed form, of the values of the measured steady-state NOEs from residue Val 60 to residue Thr 66. This decrease matches the pattern of increasing longitudinal and transverse relaxation times that was seen for both forms of SH2. The estimated error was determined using the rms noise value of regions of the spectra that contained no signal. The average error for the uncomplexed form of SH2 is 3.2%; for the complexed form, the value was 8.1%. These values are comparable to those seen by other investigators (Akke et al., 1993).

Estimation of the Overall Correlation Time τ_m. Equation 9 assumes that the overall tumbling motion of the molecule is isotropic. The validity of this assumption for the SH2 domain may be assessed by determining the principal components of the inertia tensor derived from coordinates of the preliminary PLCγ1C SH2 domain structure shown in Figure 2. The relative values were determined to be 1.00: 0.93:0.66 and suggest, therefore, that the SH2 domain may be modeled as a prolate ellipsoid. On the basis of the preliminary structure, an axial ratio of the ellipse, defined as the ratio of the long to the short semiaxes, of 1.35 is calculated. The rotational correlation times for orientation about these axes, relative to that of a sphere of equal volume, were determined using standard expressions (Cantor & Schimmel, 1980), and values of 1.12 and 1.00 were calculated for

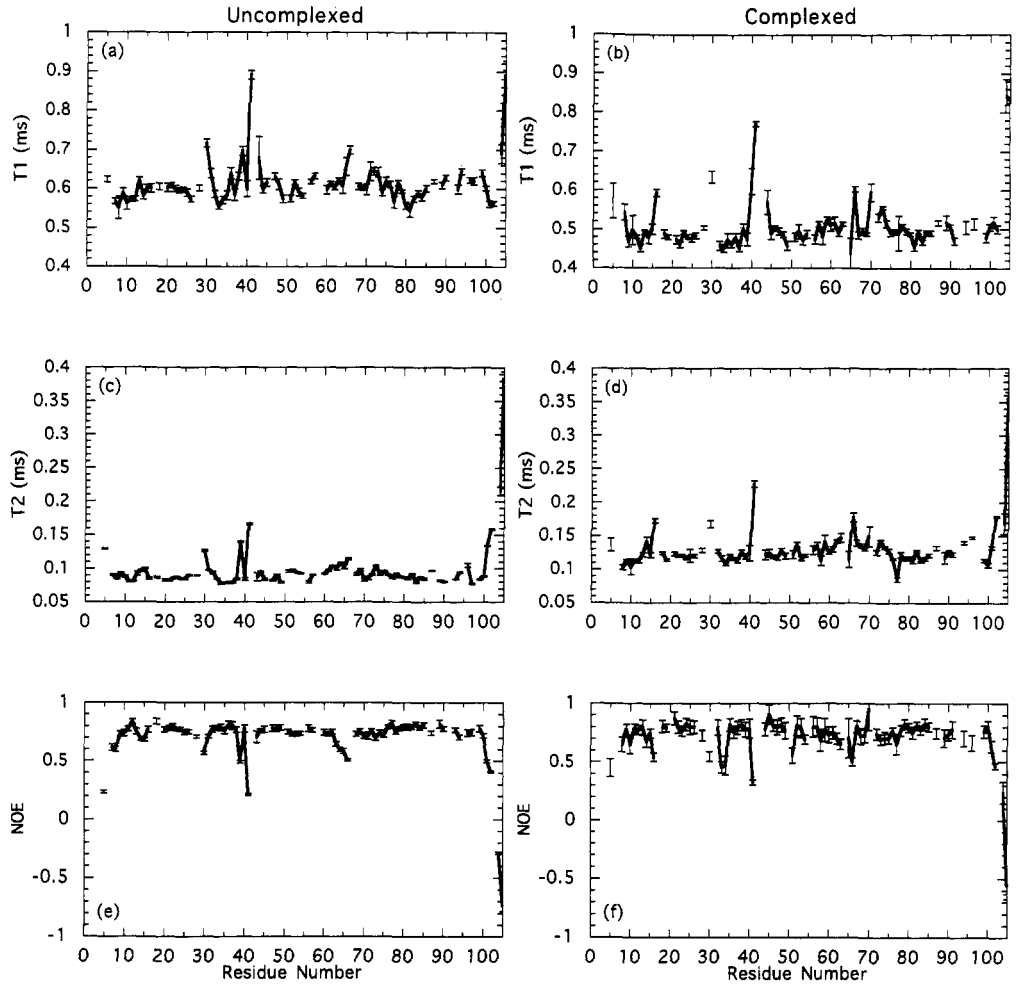

FIGURE 6: Plots of T_1, T_2, and NOE as a function of residue number. Measured T_1 values are shown in panels a and b, T_2 values are shown in panels c and d, and ^1H–^{15}N NOE data are shown in panels e and f. Panels a, c, and e refer to data for the uncomplexed form of SH2. Data for the complexed form are shown in panels b, d, and f.

reorientation about the short and long semiaxes, respectively. This strongly suggests that the assumption of isotropic rotation is valid.

Using coordinates derived from the X-ray structure of uncomplexed and complexed forms of Src SH2 (Waksman et al., 1993) to determine principal components of the inertia tensor, values of 1.00:0.86:0.60 were obtained for the uncomplexed form and values of 1.00:0.90:0.67 were obtained for the complexed form. The values obtained for the complexed PLCγ1C and Src SH2 domains are thus in good agreement, and from the Src-derived data, it is to be expected that the assumption of isotropic rotation is also valid for the uncomplexed PLCγ1C SH2 domain.

As described earlier, estimates of the overall correlation time τ_m may be determined from the T_1/T_2 ratio for each residue when certain precautions are taken. All residues with T_1/T_2 ratios greater than one standard deviation from the mean were discarded in initial evaluations of τ_m. In the uncomplexed form of SH2, eight residues had a T_1/T_2 ratio one standard deviation above the mean while seven had values one standard deviation below it. In the complexed form, seven residues were excluded as their T_1/T_2 ratios were one standard deviation above the mean. Similarly, 10 residues were excluded as they had a T_1/T_2 ratio one standard deviation below the mean. The average calculated τ_m was 9.3 ± 0.4 ns for the uncomplexed form of SH2 and 6.7 ± 0.2 ns for the peptide-complexed form, with the given errors representing standard deviations calculated over all residues considered.

A further investigation was performed to determine the overall correlation time. The T_1, T_2, and NOE relaxation parameters of the same residues that were used above were fit using the spectral density function given in eq 9. A grid search was performed for the variable τ_m, while S^2 and τ_e were optimized for individual residues. The average optimum τ_m was determined to be 9.2 ± 0.4 ns for the uncomplexed form of SH2 and 6.6 ± 0.3 ns in the peptide-complexed form—in good agreement with the values determined from the T_1/T_2 ratio alone.

Following the determination and assignment of appropriate spectral density function models for each residue, the overall correlation time was again optimized. In this analysis, the optimum τ_m value was determined for all residues simultaneously using a grid search of the variable τ_m while optimizing the parameters of the assigned spectral density functions for each residue. The optimum value was determined to be 9.2 and 6.5 ns for the uncomplexed and complexed forms, respectively.

Hydrodynamic theory predicts that the overall correlation time of an isotropically tumbling spherical molecule should be proportional to the volume of the molecule (Cantor & Schimmel, 1980; Venable & Pastor, 1988). Binding of the comparatively small peptide should change the volume of the SH2 domain only slightly and is therefore unlikely to account for the observed difference in τ_m. The very different values of τ_m seen for the two forms of SH2 are thus somewhat surprising, leading us to perform hydrodynamic measurements

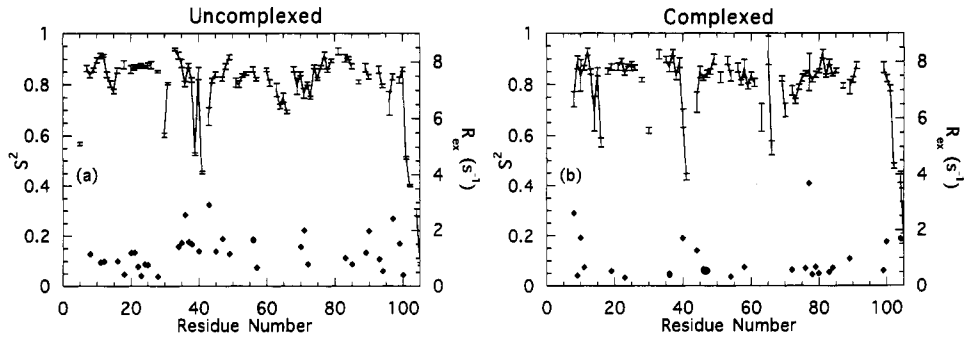

FIGURE 7: Plot of the order parameter S^2 (solid line) and R_{ex} (solid diamonds) as a function of residue number for (a) the uncomplexed form of SH2 and (b) the complexed form of SH2.

Table 1: Summary of Spectral Density Models Used To Fit T_1, T_2, and NOE Data for the Two Forms of the SH2 Domain

parameters optimized	uncomplexed SH2	complexed SH2
S^2	4	29
S^2 and τ_e	14	10
S^2 and R_{ex}	11	20
S^2, τ_e, and R_{ex}	25	5
S_s^2, S_f^2, and τ_s	24	7
not fit	4	9

on the two states of the SH2 in order to unambiguously define the oligomerization state(s) for each (see below).

Model-Free Analysis. As described above, the relaxation parameters of each residue were fit using the different spectral density functions given in eqs 9 and 10. An exchange parameter was also included with single-time-scale spectral density functions to determine if it improved the fit to the relaxation data. The optimum spectral density models were chosen as described above, and Table 1 summarizes the number of residues which fall within each class of model. The relaxation parameters could be fit within experimental errors for all but four residues (Gly 32, Gln 62, Leu 80, Ser 82) in the uncomplexed form of SH2. In the peptide-complexed form, spectral density functions that were able to fit the measured relaxation data could not be determined for nine residues: Ile 5, Gly 32, Phe 34, Glu 52, Gln 62, Val 67, Met 68, Lys 94, and Tyr 96.

Examination of Table 1 shows that the models required to fit the relaxation data were quite different for the two forms of SH2. In the uncomplexed form of SH2, an exchange term was required to fit the relaxation data of 36 residues and the two-time-scale spectral density function was invoked for 24 residues. In contrast, 25 residues in the complexed form required an exchange parameter, and the two-time-scale spectral density function was invoked for only seven residues. Simpler spectral density functions including S^2 alone, or S^2 and τ_e, were used for 18 residues in the uncomplexed form and 39 residues in the complexed form. The optimized model-free dynamics parameters and the values of the exchange term are given in Table 2. The calculated values of the generalized order parameter S^2 and the values of R_{ex} are plotted for the two forms of SH2 in Figure 7.

Generalized Order Parameter S^2. The average value of the order parameter S^2, over all residues, is 0.80 for both forms of SH2. There are a number of regions in the uncomplexed form of SH2 that appear to be more disordered on a picosecond-time scale than the average. These regions include residues Ile 5, Arg 30, Arg 39, Glu 41, and Asn 43, residues between Glu 63 and Thr 66, and the C-terminal region from residue Glu 101 to Ser 105. In the peptide-complexed form, the residues that exhibit markedly higher than average disorder include Ser 8, Ala 14, Leu 16, Arg 30, Asn 40, Glu 41, Ser 44, Glu 63, Thr 66, and Gly 70 and the C-terminal region from Glu 101 onwards. In both forms of SH2, a gradual, nonmonotonic increase is seen in the order parameter between residues 70 and 80. The overall trends in the order parameter appear to be similar between the two forms of SH2. Average order parameters calculated over different secondary structural elements are given in Table 3.

Effective Correlation Time τ_e. A τ_e parameter was necessary to fit the relaxation data throughout most of the uncomplexed form of SH2. Exceptions to this observation occur between residues Arg 50 and Lys 56 and between residues Ile 81 and Leu 89. In contrast, a large number of residues which were fit with $\tau_e > 20$ ps in the uncomplexed form no longer require the inclusion of this parameter in the complexed form. Only two regions in the complexed protein appear to have a requirement for τ_e terms, these being residues between Ser 72 and Asp 75 and between His 87 and Tyr 90.

Conformational Exchange Parameter R_{ex}. The pattern of residues requiring a nonzero R_{ex} parameter is quite different for the two forms of SH2. As noted earlier, the R_{ex} parameter was included for almost twice as many residues in the uncomplexed form as in the complexed form. The average value of the R_{ex} term for those residues which require one is 1.22 and 0.97 s^{-1} in the uncomplexed and complexed forms, respectively. There are a number of regions in the protein, for example, between residues Glu 20 and Leu 25 or between Phe 34 and Lys 38, where R_{ex} terms are required for every residue in the uncomplexed form and only very sparsely in the complexed form.

Two-Time-Scale Spectral Density Functions. In the uncomplexed form of SH2, five residues (Gln 61, Glu 63, Gly 64, Leu 69, Glu 73), in the region corresponding to the smaller β-sheet (residues Gln 61–Phe 74), required a two-time-scale spectral density function. All five residues are fit with a $\tau_s > 0.5$ ns. In the complexed form, only two residues (Glu 63 and Thr 66) within this region required a two-time-scale spectral density function. In the uncomplexed form, all residues corresponding to the CD loop and the residues adjacent to it (Ala 51–Lys 54) required the two-time-scale spectral density function. None of the corresponding residues in the complexed form required a two-time-scale model. Similarly, in the uncomplexed form, residues Arg 39, Glu 41, and Ser 44, in the BC loop, require a two-time-scale model, while only residue Glu 41 requires such a spectral density function in the peptide-complexed form.

Hydrodynamic Measurements. Figure 8 shows molecular weight vs concentration plots of PLCγ1C SH2, with and without the pY1021 peptide, as determined from equilibrium centrifugation measurements. The molecular weight vs concentration profile for uncomplexed SH2 determined from

Table 2: Values of Model-Free Parameters and R_{ex} Terms Calculated for the (A) Uncomplexed PLCγ1C SH2 and (B) Complexed PLCγ1C SH2[a]

A. Uncomplexed PLCγ1C SH2

residue	S^2	std	τ_e	std	R_{ex}	std	τ_s	std	S_f^2	std
Ile 5	0.57	0.01					0.85	0.03	0.84	0.01
His 6										
Glu 7	0.86	0.01					0.60	0.24	0.95	0.02
Ser 8	0.84	0.01	0.09	0.01	1.15	0.17				
Lys 9	0.86	0.01	0.04	0.01						
Glu 10	0.90	0.01	0.04	0.02						
Trp 11	0.91	0.01	0.02	0.01	0.86	0.25				
Tyr 12	0.91	0.00			0.89	0.11				
His 13	0.84	0.01	0.02	0.01						
Ala 14	0.80	0.01					1.29	0.26	0.88	0.01
Ser 15	0.77	0.01					1.22	0.17	0.86	0.01
Leu 16	0.86	0.01	0.01	0.01	0.90	0.27				
Trp 17										
Arg 18	0.88	0.02			0.43	0.24				
Ala 19										
Gln 20	0.86	0.01	0.01	0.01	1.19	0.32				
Ala 21	0.87	0.01	0.01	0.01	1.21	0.16				
Glu 22	0.87	0.01			0.71	0.13				
His 23	0.88	0.01	0.01	0.01	0.37	0.10				
Met 24	0.87	0.00	0.01	0.01	0.80	0.09				
Leu 25	0.88	0.01	0.03	0.01	0.75	0.21				
Met 26	0.88	0.01					1.01	0.62	0.91	0.03
Arg 27										
Val 28	0.85	0.00	0.04	0.01	0.34	0.08				
Arg 30	0.60	0.01					1.04	0.07	0.72	0.00
Asp 31	0.81	0.00	0.03	0.00						
Gly 32										
Ala 33	0.94	0.00	0.02	0.02						
Phe 34	0.91	0.01			1.41	0.30				
Leu 35	0.88	0.02	0.02	0.01	1.55	0.23				
Val 36	0.80	0.01			2.56	0.27				
Arg 37	0.87	0.01			1.58	0.22				
Lys 38	0.82	0.01	0.01	0.01	1.50	0.17				
Arg 39	0.53	0.00					1.25	0.04	0.71	0.00
Asn 40	0.84	0.02	0.01	0.01	1.26	0.38				
Glu 41	0.45	0.00					0.61	0.04	0.62	0.00
Asn 43	0.68	0.04	0.01	0.01	2.93	0.83				
Ser 44	0.82	0.01					1.82	0.77	0.86	0.02
Tyr 45	0.84	0.01	0.01	0.01	1.26	0.21				
Ala 46										
Ile 47	0.82	0.01	0.01	0.01	1.70	0.14				
Ser 48	0.87	0.01	0.01	0.01						
Phe 49	0.91	0.01			1.16	0.21				
Arg 50										
Ala 51	0.81	0.02					2.21	0.89	0.87	0.01
Glu 52	0.80	0.01					1.23	0.42	0.85	0.02
Gly 53	0.84	0.01					1.07	0.45	0.88	0.01
Lys 54	0.84	0.01					1.32	0.40	0.89	0.01
Ile 55										
Lys 56	0.86	0.01			1.68	0.31				
His 57	0.82	0.01	0.01	0.01	0.67	0.11				
Cys 58										
Arg 59										
Val 60	0.86	0.01	0.03	0.01						
Gln 61	0.81	0.01					1.22	0.42	0.85	0.01
Gln 62										
Glu 63	0.78	0.03					0.78	0.35	0.85	0.05
Gly 64	0.71	0.01					1.00	0.12	0.82	0.01
Gln 65	0.75	0.02	0.05	0.01						
Thr 66	0.69	0.01	0.06	0.00						
Val 67										
Met 68	0.86	0.01	0.03	0.01						
Leu 69	0.79	0.03					2.03	1.11	0.85	0.03
Gly 70	0.84	0.01	0.04	0.01	1.41	0.33				
Asn 71	0.77	0.02	0.02	0.01	2.01	0.44				
Ser 72	0.80	0.01	0.01	0.00	0.79	0.16				
Glu 73	0.75	0.01					1.00	0.32	0.81	0.03
Phe 74	0.87	0.01	0.03	0.01						
Asp 75	0.82	0.01	0.03	0.01						
Ser 76	0.87	0.01								
Leu 77	0.92	0.01								
Val 78	0.86	0.01	0.02	0.01						
Asp 79	0.89	0.01	0.01	0.01						
Leu 80										
Ile 81	0.93	0.01								

Table 2 (Continued)

A. Uncomplexed PLCγ1C SH2

residue	S^2	std	τ_e	std	R_{ex}	std	τ_s	std	S_f^2	std
Ser 82										
Tyr 83	0.90	0.01			1.01	0.28				
Tyr 84	0.90	0.01								
Glu 85	0.87	0.01			0.79	0.24				
Lys 86										
His 87	0.81	0.01					1.10	0.47	0.85	0.01
Leu 89	0.87	0.02			1.20	0.27				
Tyr 90	0.83	0.01	0.01	0.01	1.99	0.20				
Arg 91										
Lys 92										
Met 93	0.86	0.01	0.02	0.01	0.98	0.19				
Lys 94	0.80	0.01	0.03	0.01	0.54	0.13				
Leu 95										
Arg 96	0.73	0.05					2.60	1.25	0.81	0.04
Tyr 97	0.83	0.01	0.02	0.01	2.42	0.19				
Ile 99	0.82	0.01	0.01	0.01	1.52	0.17				
Asn 100	0.86	0.01	0.04	0.01	0.40	0.14				
Glu 101	0.51	0.00					1.72	0.05	0.82	0.01
Glu 102	0.40	0.00					1.69	0.03	0.79	0.00
Asn 103										
Ser 104	0.29	0.01					0.82	0.03	0.74	0.01
Ser 105	0.09	0.01					0.82	0.01	0.75	0.01

B. Complexed PLCγ1C SH2

residue	S^2	std	τ_e	std	R_{ex}	std	τ_s	std	S_f^2	std
Ile 5										
His 6										
Glu 7										
Ser 8	0.74	0.03	0.04	0.02	2.62	0.37				
Lys 9	0.89	0.03			0.39	0.25				
Glu 10	0.84	0.06			1.74	1.27				
Trp 11	0.87	0.01			0.69	0.13				
Tyr 12	0.93	0.01								
His 13	0.85	0.01								
Ala 14	0.69	0.07					2.26	1.84	0.85	0.04
Ser 15	0.85	0.02								
Leu 16	0.57	0.02					1.11	0.22	0.72	0.01
Trp 17										
Arg 18	0.85	0.01								
Ala 19	0.87	0.01			0.55	0.18				
Gln 20										
Ala 21	0.87	0.01								
Glu 22	0.89	0.01								
His 23	0.85	0.01			0.31	0.17				
Met 24	0.88	0.00								
Leu 25	0.87	0.02								
Met 26	0.87	0.01								
Arg 27										
Val 28	0.82	0.01	0.02	0.02						
Arg 30	0.62	0.01	0.04	0.01						
Asp 31										
Gly 32										
Ala 33	0.92	0.02								
Phe 34										
Leu 35	0.90	0.01								
Val 36	0.87	0.02			0.44	0.22				
Arg 39	0.93	0.01								
Lys 38	0.83	0.01								
Arg 39	0.89	0.02								
Asn 40	0.67	0.04			1.72	0.77				
Glu 41	0.44	0.01					0.64	0.11	0.59	0.00
Asn 43										
Ser 44	0.73	0.04			1.27	0.60				
Tyr 45	0.85	0.02								
Ala 46	0.83	0.01			0.60	0.17				
Ile 47	0.84	0.01			0.53	0.30				
Ser 48	0.85	0.01								
Phe 49	0.90	0.02								
Arg 50										
Ala 51	0.83	0.02	0.12	0.04						
Glu 52										
Gly 53	0.89	0.02								
Lys 54	0.83	0.02	0.05	0.02	0.34	0.23				
Ile 55										
Lys 56	0.87	0.02								
His 57	0.81	0.01								

Table 2 (Continued)

	B. Complexed PLCγ1C SH2									
residue	S^2	std	τ_e	std	R_{ex}	std	τ_s	std	S_f^2	std
Cys 58	0.86	0.04			0.67	0.67				
Arg 59	0.79	0.01								
Val 60	0.83	0.01								
Gln 61	0.81	0.02								
Gln 62										
Glu 63	0.67	0.05					1.70	0.85	0.81	0.03
Gly 64										
Gln 65	0.93	0.05								
Thr 66	0.55	0.03					1.06	0.21	0.72	0.01
Val 67										
Met 68										
Leu 69	0.82	0.01	0.05	0.02						
Gly 70	0.70	0.03								
Asn 71										
Ser 72	0.78	0.02	0.01	0.01	0.57	0.26				
Glu 73	0.73	0.01	0.02	0.01						
Phe 74	0.79	0.01	0.03	0.02						
Asp 75	0.83	0.01	0.04	0.02						
Ser 76	0.84	0.01			0.63	0.16				
Leu 77	0.85	0.07			3.68	0.84				
Val 78	0.82	0.01			0.42	0.26				
Asp 79	0.84	0.01			0.68	0.15				
Leu 80	0.85	0.01			0.46	0.21				
Ile 81	0.92	0.02								
Ser 82	0.83	0.01								
Tyr 83	0.89	0.01			0.50	0.15				
Tyr 84	0.84	0.00			0.66	0.20				
Glu 85	0.85	0.01								
Lys 86										
His 87	0.80	0.01	0.02	0.01						
Leu 89	0.79	0.03	0.03	0.03	0.98	0.55				
Tyr 90	0.82	0.01	0.02	0.02						
Arg 91	0.88	0.01								
Lys 92										
Met 93										
Lys 94										
Leu 95										
Arg 96										
Tyr 97										
Ile 99	0.87	0.02			0.55	0.28				
Asn 100	0.82	0.01			1.58	0.31				
Glu 101	0.79	0.01	0.06	0.02						
Glu 102	0.48	0.01					1.70	0.13	0.82	0.02
Asn 103										
Ser 104	0.43	0.02	0.05	0.01	1.69	0.57				
Ser 105	0.19	0.01					0.66	0.04	0.64	0.01

[a] The correlation times τ_e and τ_s are expressed in nanoseconds. R_{ex} is expressed in inverse seconds. Note: Residues Gly 1 and Ser 2 were unassigned. Due to rapid amide–water exchange, resonances of Gly 4 were not observed. Prolines 3, 29, 42, 88, and 98 are not listed in the table.

light-scattering results is also illustrated. The calculated molecular weights of the free and complexed SH2 are 12 260 and 13 720 Da, respectively. At all concentration ranges examined, the measured values for the molecular weight of the free SH2 domain are higher than expected and significantly larger than the measured molecular weights of the SH2-pY1021 complex. In contrast, the measured weight values for the complex are in agreement with the calculated weight at any of the concentrations examined.

DISCUSSION

Overall Correlation Time. The overall correlation times that have been determined for the two forms of SH2 differ significantly from each other. Other studies have determined overall correlation times for proteins of a variety of sizes (Kay et al., 1989; Stone et al., 1992, 1993; Kördel et al., 1992; Palmer et al., 1991; Clore et al., 1990a). Since the overall correlation time of a molecule should be approximately proportional to its molecular weight, the measured value of 6.5 ns for the peptide-complexed form of SH2 is in agreement with the literature. The higher value of 9.2 ns that is seen for the uncomplexed form is surprising. On the basis of our calculations of the principal components of the inertia tensor from the X-ray structures of uncomplexed and peptide-complexed Src SH2 (Waksman et al., 1993), the overall shape of the SH2 domain does not change dramatically upon binding the peptide. Therefore, binding of the peptide alone can not account for the change in the overall correlation time. The most likely explanation for the higher than expected correlation time is that the sample contains an equilibrium of monomeric and dimeric forms of the SH2 domain, and therefore, the correlation time of 9.2 ns is that of a population-weighted average. Hydrodynamic measurements, summarized in Figure 8 and including sedimentation equilibrium ultracentrifugation and light-scattering data, indicate that the uncomplexed form of PLCγ1C SH2 has a propensity to aggregate at concentrations as low as 2–4 mg/mL, well under the concentration used in the NMR studies (12–18 mg/mL). The weight-averaged molecular weight calculated by centrifugation for the uncomplexed SH2 domain at a concentration of 6.5 mg/mL is approximately 20% larger than that measured for the SH2-pY1021 complex. In addition, light-scattering results

Table 3: Average Order Parameter Values for Secondary Structural Elements[a]

		uncomplexed SH2		complexed SH2	
structural element	residues considered	components	totals	components	totals
helix A					
αA	17–28		[9] 0.87 (0.01)		[9] 0.86 (0.02)
large β-sheet					
βB	33–38	[6] 0.87 (0.05)		[5] 0.89 (0.04)	
βC	45–51	[5] 0.85 (0.04)	[15] 0.86 (0.04)	[6] 0.85 (0.03)	[17] 0.86 (0.04)
βD	54–60	[4] 0.85 (0.02)		[6] 0.83 (0.03)	
small β-sheet					
βD′	61–63	[2] 0.79 (0.02)		[2] 0.74 (0.10)	
βE	66–69	[3] 0.78 (0.08)	[8] 0.79 (0.06)	[2] 0.69 (0.20)	[7] 0.74 (0.10)
βF	72–74	[3] 0.81 (0.06)		[3] 0.77 (0.03)	
helix B					
αB	77–87		[8] 0.88 (0.04)		[9] 0.85 (0.04)
loops					
AA	14–16	[3] 0.81 (0.04)		[3] 0.70 (0.14)	
AB	29–32	[2] 0.70 (0.14)		[1] 0.62	
BC	39–44	[5] 0.66 (0.17)		[4] 0.68 (0.19)	
CD	52–53	[2] 0.82 (0.02)	[21] 0.76 (0.11)	[1] 0.89	[14] 0.75 (0.14)
DE	64–65	[2] 0.73 (0.02)		[1] 0.93	
EF	70–71	[2] 0.80 (0.05)		[1] 0.70	
BG	88–96	[5] 0.82 (0.06)		[3] 0.83 (0.04)	

[a] Number of residues for which data were available is noted in square brackets. Standard deviations are given in parentheses.

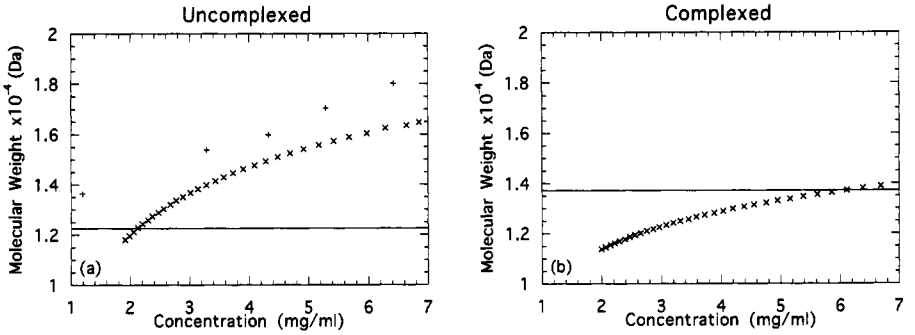

FIGURE 8: Plots of apparent molecular weight against concentration from light-scattering studies (+) and sedimentation equilibrium studies (×) for (a) uncomplexed PLCγ1C SH2 and (b) PLCγ1C SH2 in complex with pY1021 peptide. The expected molecular weights of the SH2 domain alone (12 260 Da) and in complex with peptide (13 720 Da) are indicated by the solid horizontal lines in the respective figures.

also provide clear evidence of concentration-dependent aggregation of the uncomplexed SH2 domain.

Because of the monomer–dimer equilibrium in the uncomplexed SH2 sample, the measured relaxation rates and steady-state NOEs reflect a combination of both of these oligomeric states. Care should be taken, therefore, when comparing relaxation parameters of the uncomplexed SH2 to those of the purely monomeric complexed form. T_1, T_2, and NOE measurements at a single field strength do not provide enough data to permit determination of separate model-free dynamics parameters for the monomeric and dimeric states. As a result, the model-free dynamics parameters that were determined for the uncomplexed form of SH2 characterize a combination of the two oligomeric states. In what follows, it must be understood that a comparison of the dynamics parameters of uncomplexed and complexed SH2 is in fact a comparison of the parameters which reflect a composite of monomer and dimer internal dynamics in the case of the uncomplexed SH2 with the dynamics parameters of a monomeric complex of SH2 and pY1021 peptide.

Backbone Dynamics of Uncomplexed SH2. Both the N- and C-terminal regions of the PLCγ1C SH2 domain appear to exhibit considerable disorder. Amide resonances of the first two residues, Gly 1 and Ser 2, were not assigned, most likely due to extremely rapid amide exchange with solvent, leading to the disappearance of these resonances. Since residue 3 is a proline, no amide relaxation data could be measured. Gly 4 exhibited significant amide NH exchange with water, leading to very weak correlation peaks in the relaxation spectra. These observations in themselves suggest that the N-terminal region of the protein is disordered. The most N-terminal residue of the protein for which an order parameter could be calculated was Ile 5, with an S^2 of 0.57 ± 0.01, indicating that it exhibits considerable disorder on a picosecond-time scale. Similarly, residues 101–105 in the C-terminal region of the protein all have low order parameters, indicating that this region is disordered on a picosecond-time scale. This result is not particularly surprising, since the first five and last three residues of the fragment we are studying are derived from the plasmid sequences rather than from native SH2 sequences, and therefore, we would not expect stable secondary structures in these regions. Our observation that the terminal regions of the protein are disordered is also consistent with results from similar studies on a number of other proteins (Stone et al., 1992, 1993; Barbato et al., 1992; Clore et al., 1990a; Kördel et al., 1992; Akke et al., 1993; Schneider et al., 1992).

We examined the correlation between the value of the generalized order parameter and the different elements of secondary structure. Other similar analyses appear to reflect a dependence on the protein under study. The analysis of staphylococcal nuclease (Kay et al., 1989) revealed no correlation between the value of a residue's order parameter and the localization of that residue in either α-helices, β-sheets, turns, or loops. Analysis of apo- and ion-bound states of

calbindin (Kördel et al., 1992; Akke et al., 1993) showed that the 10-residue "linker loop" exhibited markedly lower order parameters. Similarly, five residues in the center of the linker helix connecting the N- and C-terminal globular domains in calmodulin were shown to exhibit high mobility, as were two smaller loops between the EF hands in each domain (Barbato et al., 1992). Other studies of the glucose permease IIA domain (Stone et al., 1993) and interleukin-1β (Clore et al., 1990a) have revealed lower order parameters in certain loops between β-strands. However, in both proteins, a correlation was not found for all such loops.

In Table 3, we list the average order parameters for the different secondary structural elements of the SH2 domain. The average values for the α-helices, 0.87 ± 0.01 (helix A) and 0.88 ± 0.04 (helix B), are comparable to those found in other studies (Kördel et al., 1992; Kay et al., 1989). The two β-sheets have slightly lower order parameters than the helices, 0.86 ± 0.04 and 0.79 ± 0.06, for the large and small sheets, respectively. These values are similar to the values determined for the β-sheet of the glucose permease IIA domain, 0.81 ± 0.06 (Stone et al., 1992), and β-sheets in staphylococcal nuclease, 0.86 ± 0.04 (Kay et al., 1989), and to the overall average value of 0.82 ± 0.05 determined for the predominantly β-strand structure of interleukin-1β (Clore et al., 1990a).

The average value of the order parameter determined for the loop and turn structures in the uncomplexed SH2 is 0.76 ± 0.11. This value is lower than the value of 0.86 ± 0.04 determined for loops in staphylococcal nuclease (Kay et al., 1989) but is considerably higher than the value of 0.59 ± 0.23 determined for the 10-residue linker loop in Ca^{2+}–calbindin (Kördel et al., 1992). A more detailed analysis of which residues contribute most to lowering the average order parameter in the loop and turn regions of the uncomplexed SH2 domain reveals that the highly disordered residues are associated with only a few loop and turn structures. For example, Ser 15 (AA loop) and Arg 30 (AB loop) have S^2 values of 0.77 and 0.60, respectively. Three residues of the BC loop, Arg 39, Glu 41, and Asn 43, have lower than average order parameters. Similarly, residues Gly 64 and Gln 65, which lie in the turn between strands βD′ and βE, and Thr 66, the first residue of strand βE, all have low order parameters. Our observation that some, but not all, loop structures have lower order parameters is similar to that made for interleukin-1β (Clore et al., 1990a).

Correlations between the order parameters and crystallographic B-factors have also been examined. The study of staphylococcal nuclease (Kay et al., 1989) reported no such correlation, while the study of interleukin-1β (Clore et al., 1990a) reported some correlation, most notably in two loop regions, and Kördel et al. (1992) reported a fairly strong correlation between the order parameters and B-factors in Ca^{2+}–calbindin. It was of interest to determine the degree of correlation between regions of high B-factors in previously published X-ray structures of SH2 domains and lower order parameters determined from our relaxation data. Because X-ray crystallographic structural data are not available for the PLCγ1C SH2 domain, we compared our results to data from the homologous Src SH2 domain (Waksman et al., 1993). The uncomplexed form of Src SH2 has four molecules in its asymmetric unit cell, all of which exhibit above average temperature factors in regions corresponding to the BC, CD, and DE loops. These observations correlate well with the lower order parameters that are observed for the BC and DE loops in the uncomplexed PLCγ1C SH2 domain. However, lower than average order parameters are not observed for the CD loop. A reasonable explanation for this discrepancy is the difference in the length of this loop in the Src and PLCγ1C SH2 domains. In the PLCγ1C SH2 domain, the CD loop is just two residues long, while in Src SH2, the increased length of the loop (seven residues) may permit greater conformational freedom. Overall, the level of correlation between order parameters and B-factors that we observe is similar to that which was seen in interleukin-1β, namely that a correlation seems to exist for some but not all loop structures.

Studies of calbindin (Akke et al., 1993) have correlated the requirement for an R_{ex} term with exchange between different conformations in certain regions of the molecule. For PLCγ1C SH2, the number of residues requiring an R_{ex} term, the range of R_{ex} values, and their distribution is similar to that seen in interleukin-1β (Clore et al., 1990a). The pattern of residues requiring an R_{ex} term does not appear to be strongly correlated with secondary structural type in PLCγ1C SH2. Similar secondary structural elements exhibit quite different requirements for a line-broadening term; for example, helix αA requires exchange terms for all but one residue from Arg 18 to Leu 25, while helix αB requires only two R_{ex} terms, for Tyr 83 and Glu 85. In the uncomplexed form of PLCγ1C SH2, there are three distinct regions that appear to require R_{ex} terms, including seven of the 12 residues of helix αA, residues 34–38 in strand βB, and four residues in the BG loop. A requirement for R_{ex} terms at the beginning and end of secondary structural elements, which was observed for interleukin-1β (Clore et al., 1990a), is not seen in PLCγ1C SH2. However, we note that of the 24 residues requiring a two-time-scale spectral density function, many lie at, or close to, the ends of secondary structural elements. Interestingly, residue Gln 61, which lies at the transition between strands βD and βD′, is one of the few residues lying within a secondary structural element that requires a two-time-scale spectral density function.

Sixty residues of the uncomplexed PLCγ1C SH2 require either an R_{ex} term or a two-time-scale spectral density function to fit the measured relaxation data. This observation suggests that there is a significant amount of motion within the molecule on time scales slower than the picosecond-time scale characterized by the order parameter S^2. The implications of these requirements are discussed more fully below in the context of changes that occur upon peptide binding.

Backbone Dynamics of SH2 Domain Complexed with the pY1021 Peptide. Overall, many of the general observations that are made for the uncomplexed form of SH2 are also true for the peptide-complexed form. Broadly, similar levels of correlation are seen between the order parameters and both the secondary structural elements and the crsytallographic B-factors for the two forms of SH2.

As in the uncomplexed SH2 domain, the N- and C-terminal regions of complexed SH2 appear to be highly disordered. Both the N- and C-terminal regions are situated on the opposite side of the main β-sheet to that occupied by the complexed peptide. As a result, it is highly unlikely that they would be involved in, or affected by, recognition and binding of the peptide.

Many of the residues exhibiting lower order parameters are associated with, or are close to, loop structures. As was seen in the uncomplexed form of SH2, a number of residues in the BC loop (Asn 40, Glu 41, Ser 44) exhibit a high degree of mobility on picosecond-time scales. Residues Glu 63 (S^2 = 0.67 ± 0.05) and Thr 66 (S^2 = 0.55 ± 0.03), which are adjacent to the DE loop, exhibit low order parameters in the complexed SH2, but residue Gln 65, which exhibits a high

degree of mobility in the uncomplexed form, now is restricted ($S^2 = 0.93 \pm 0.05$). Residue Arg 30, in the center of the AB loop, appears to be somewhat disordered ($S^2 = 0.62 \pm 0.01$), as found in the uncomplexed form. In the AA loop, residues Ala 14 and Leu 16 exhibit high mobility which is not seen in the uncomplexed data whereas Ser 15 appears to lose mobility upon binding the peptide. Therefore, we conclude that while the same loops are associated with lower order parameters, the individual residues manifesting this high mobility differ in the two forms of SH2.

Changes in Backbone Dynamics upon Peptide Binding. One of the major motivations for the study described here is to examine changes in the dynamic behavior of the SH2 domain that occur upon binding the peptide. A number of similar studies have examined binding-induced changes in dynamics; these include the effects of binding the inhibitor pdTp and the ligand Ca^{2+} on the dynamics of staphylococcal nuclease leucine methyl carbons (Nicholson et al., 1992) and the changes in calbindin dynamics upon binding Ca^{2+} and Cd^{2+} ions (Kördel et al., 1992; Akke et al., 1993). In the case of staphylococcal nuclease, it was shown that the mean-squared order parameters associated with the reorientation of the C^{γ}–C^{δ} bond axis increase exclusively in those regions within 10 Å of either the Ca^{2+} or pdTp heavy atoms. Similarly, Akke et al. (1993) showed that for the second binding loop in calbindin there was a marked increase in the average order parameter upon ion binding. In contrast, the N-terminal loop of calbindin, which does not have low order parameters in the apo form, showed little change in the order parameters upon metal binding.

The results of these two studies have suggested that ligand binding induces a localized stiffening of the protein structure in regions near the binding sites. In both of the previous studies, the bound ligand was small relative to the 12-residue peptide ligand that we are considering here. Previous studies of the Lck SH2 domain in complex with high-affinity peptide have shown that seven residues of the peptide, including the phosphotyrosine, are involved in contacts with the SH2 domain and that the total area of interaction is approximately 500 Å^2 (Eck et al., 1993). Because the size and the region of interaction of the ligand in our study are much larger than those in the calbindin and staphylococcal nuclease studies, we were interested in examining whether a similar stiffening of structure occurred throughout the larger binding site of the SH2 domain upon peptide binding.

At present, high-resolution structures of the PLCγ1C SH2 domain are not available for either the peptide-complexed or free forms. Therefore, indirect evidence and references to analogous structures must be used to postulate which residues are likely to be integral to binding the peptide. The published structures of the Lck (Eck et al., 1993) and Src (Waksman et al., 1993) SH2 domains in complex with an identical 11-residue peptide reveal very similar binding configurations, in which two residues of the peptide, the phosphotyrosine and the isoleucine three residues C-terminal to it, are located in two separate pockets of the protein. The phosphotyrosine-binding site is comprised of residues from strands βB and βD, from helix αA, and from the BC loop. Comparison of the free and complexed forms of SH2 shows that the major structural change that occurs upon peptide binding in this region is that the BC loop folds over the phosphotyrosine and becomes less disordered. The second major interaction site, a hydrophobic pocket which encloses the isoleucine, is formed by loops EF and BG in conjunction with residues from helix αB and strand βD. In contrast to the phosphotyrosine site, this pocket appears to become more open upon binding the peptide.

Indirect evidence as to which residues in the PLCγ1C SH2 domain are involved in binding the peptide comes from peptide titration studies. These studies have shown that the following residues exhibit an ^{15}N chemical shift change of greater than 0.5 ppm on binding the peptide: Ile 47, Lys 56, His 57, Cys 58, Leu 69, Glu 73, Leu 89, Tyr 90, and Lys 92. Residues which show an NH or CαH proton chemical shift change of greater than 0.6 ppm on binding include Leu 16, Arg 18, Lys 38, Ala 46, Ile 47, Ser 48, Ala 51, Ile 55, Lys 56, His 57, Cys 58, Arg 59, Val 60, Gln 61, Tyr 90, and Met 93. Although chemical shift changes are not always indicative of involvement in binding, the positions of residues exhibiting such changes correlate well with residues involved in binding in the analogous structures of Lck and Src. It is therefore expected that the complexed peptide extends across strand βD of the main β-sheet of PLCγ1C, spanning from the BC loop toward helix αB. It is somewhat surprising, in relation to crystal structures of similar SH2 complexes, that significant changes in chemical shifts are not seen in the BC loop itself.

Three highly conserved residues, Lys βD6, His βD4, and Arg αA2, form the mouth of the phosphotyrosine-binding pocket in the Lck and Src SH2 domain structures, and a fourth strictly conserved residue, Arg βB5, lies at the bottom of the pocket. [Using the convention proposed by Eck et al. (1993), Lys βD6 refers to the sixth residue in strand βD, etc.] Three of these residues are conserved in PLCγ1C SH2, the exception being the replacement of a lysine at βD6 with an arginine. Relaxation data are available to permit determination of the change in order parameters upon binding for His βD4, Arg αA2, and Arg βB5. These data are collected in Table 4 along with comparative data for other PLCγ1C residues that are expected to line the phosphopeptide-binding site. The order parameters of His βD4 and Arg αA2 are not greatly influenced by peptide binding; the S^2 of His βD4 changes from 0.82 ± 0.01 to 0.81 ± 0.01 upon binding, while the S^2 of Arg αA2 changes from 0.88 ± 0.02 to 0.85 ± 0.01. Residue Arg βB5 shows a slight increase in order parameter upon binding, from 0.87 ± 0.01 to 0.93 ± 0.01. More significant changes are seen for the first two residues in the BC loop. Residue Arg 39 is analogous to a serine (Ser βB7) in the Lck and Src structures which interacts with the phosphotyrosine. The order parameter of Arg 39 increases from 0.53 ± 0.00 to 0.89 ± 0.02 upon binding. The next residue in the BC loop, Asn 40, shows a decrease in order parameter, from 0.84 ± 0.02 to 0.67 ± 0.04 upon binding, while Glu 41 appears disordered in both forms, S^2 of 0.45 ± 0.00 in the uncomplexed and S^2 of 0.44 ± 0.01 in the complexed. Two residues which do appear to exhibit a change in order parameter upon binding are residues Ala 14 and Leu 16. These two residues are located in the loop at the N-terminal region of helix αA and were not seen to interact with the phosphopeptide in X-ray crystallographic studies of Src and Lck SH2–phosphopeptide complexes (Waksman et al., 1993; Eck et al., 1993). The order parameters of both these residues indicate that they become more disordered on a picosecond-time scale upon binding the peptide. Because these residues are close to the phosphotyrosine-binding pocket, data are included under this heading in Table 4.

On the basis of the previous studies of changes in dynamics upon ligand binding, we had expected to find that the residues involved in interactions with the phosphotyrosine would exhibit increased order parameters upon binding peptide. Our results indicate this to be the case only for certain residues, while others show the opposite trend.

Table 4: Summary of the Change in Order Parameters of Residues Putatively Located in the Phosphopeptide-Binding Site of PLCγ1C

region	designation	PLCγ1C residue	uncomplexed S^2	complexed S^2	% change S^2
		Phosphotyrosine-Binding Site			
mouth	αA2	Arg 18	0.88 ± 0.01	0.85 ± 0.01	−3.4
	βD4	His 57	0.82 ± 0.01	0.81 ± 0.01	−1.2
	βD6	Arg 59	ND	0.79 ± 0.01	ND
base	βB5	Arg 37	0.87 ± 0.01	0.93 ± 0.01	6.9
BC loop	βB7[a]	Arg 39	0.53 ± 0.00	0.82 ± 0.02	54.7
	BC1	Asn 40	0.84 ± 0.02	0.67 ± 0.04	−20.2
	BC2	Glu 41	0.45 ± 0.00	0.44 ± 0.01	−2.2
AA loop	AA1	Ala 14	0.80 ± 0.01	0.69 ± 0.07	−13.7
	AA3	Leu 16	0.86 ± 0.01	0.57 ± 0.02	−33.7
		Hydrophobic Binding Site			
	βE4	Leu 69	0.79 ± 0.03	0.82 ± 0.01	3.8
	EF1	Gly 70	0.84 ± 0.01	0.70 ± 0.03	−16.7
	αB9	Tyr 84	0.90 ± 0.01	0.84 ± 0.00	−6.7
BG loop	BG2	Leu 89	0.87 ± 0.02	0.79 ± 0.03	−9.2
	BG3	Tyr 90	0.83 ± 0.01	0.82 ± 0.01	−1.2

[a] From preliminary data, this residue appears to occur not in β-strand B but in the BC loop.

The residues C-terminal to the phosphotyrosine in the peptide used in the X-ray crystallographic studies with the Src and Lck SH2s, EPQpYEEIPIYL, and those in the pY1021 peptide, DNDpYIIPLPDPK, are quite different. One consequence of this difference is that we can be less certain about which residues of the SH2 of PLCγ1C interact with the C-terminal peptide residues. However, as mentioned earlier, titration studies suggest that the peptide in PLCγ1C SH2 is bound in approximately the same manner. Residues βD3–βD6, which are analogous to those binding the two glutamates of the phosphopeptide in the Src and Lck structures, show no significant changes in order parameter upon binding the pY1021 peptide. Residues which are analogous to those interacting with the amino acid three residues C-terminal to the phosphotyrosine in the Lck and Src structures include Leu 69, Gly 70, and Tyr 84. The order parameter of Leu 69 is not changed significantly upon binding, increasing slightly from 0.79 ± 0.03 to 0.82 ± 0.01. The order parameters for Gly 70 and Tyr 84 both indicate slightly higher picosecond-time-scale disorder upon binding; S^2 for Gly 70 changes from 0.84 ± 0.01 to 0.70 ± 0.03 upon binding, while S^2 for Tyr 84 is reduced from 0.90 ± 0.01 to 0.84 ± 0.00. The other residues which interact with the peptide in the crystal structures are analogous to the second and third residues of the BG loop in PLCγ1C, Leu 89 and Tyr 90, respectively. These residues also appear to have slightly decreased S^2 values upon binding. Overall, residues in the putative hydrophobic interaction site seem to manifest slightly increased picosecond disorder in the complexed form, contrary to what might have been expected from other ligand-binding studies (Nicholson et al., 1992; Akke et al., 1993).

To summarize these observations, it does not appear that binding the peptide leads to a restriction of the picosecond disorder characterized by the order parameter S^2, as was seen for ligand binding in the calcium-binding loop II of calbindin (Akke et al., 1993). A large increase in order parameter was seen for only a single residue, Arg 39, in the region of the phosphotyrosine binding site.

The order parameter S^2 measures the extent of picosecond motions. It is also of interest to examine how slower processes on the microsecond-to-millisecond-time scale are affected by peptide binding through a comparison of R_{ex} values in the complexed and free forms. Interpretation of R_{ex} values is complicated somewhat because a residue's requirement for an R_{ex} term can arise from sources other than slow conformational exchange of the residue. Such a requirement may also arise from changes in chemical environment as a result of motion of vicinal residues. In this study, it is impossible for us to separate these effects, and as a result, we can only state that a requirement for an R_{ex} term is consistent with the presence of slow conformational exchange. In Figure 9, we illustrate which regions of the 3D structure of PLCγ1C SH2 require R_{ex} terms in the absence and presence of the phosphopeptide. The changes in requirements for R_{ex} terms in different secondary structural elements of the molecule upon binding the phosphopeptide are discussed below. Also shown in the figure are those residues which require the two-time-scale spectral density function to fit the measured relaxation data, and the changes in these requirements are also discussed below.

One striking difference is that the number of residues requiring R_{ex} terms is different in the two forms of SH2, 36 in the uncomplexed form and 25 in the complexed form. This is consistent with the uncomplexed form of SH2 having more conformational freedom as described by Waksman et al. (1993), who interpret structural differences between uncomplexed and complexed Src SH2 as an indication of increased structural flexibility in the absence of peptide. It may also represent, however, the presence of additional motions due to monomer–dimer equilibrium in the uncomplexed form. In order for a more precise evaluation of the effect of peptide binding upon backbone dynamics to be made, it will be necessary to determine order parameters for the purely monomeric form of uncomplexed SH2. To achieve this, we are currently collecting relaxation data at several different field strengths which will allow order parameters to be calculated for both oligomeric states.

The BC loop has been shown to fold over the phosphotyrosine upon binding the peptide in Src SH2 (Waksman et al., 1993) and appears to be highly mobile in the uncomplexed SH2 structure of p85αN SH2 (Booker et al., 1992). It was thus of interest to determine if residues of this loop required an R_{ex} term in the uncomplexed form and subsequently lost this requirement in the peptide-complexed state. In this loop, we have comparative data for residues Arg 39, Asn 40, Glu 41, and Ser 44. Residues Arg 39 and Glu 41 do not require an R_{ex} term in either form of SH2, Asn 40 requires an R_{ex} term in both forms of SH2, and Ser 44 requires an R_{ex} term in only the complexed form, suggesting that the microsecond-to-millisecond-time-scale motions present in this loop are not significantly affected by the binding of the peptide.

Two regions of secondary structure exhibit different requirements for R_{ex} terms in the two forms of SH2. In the uncomplexed form, residues Gln 20–Leu 25 of helix αA all

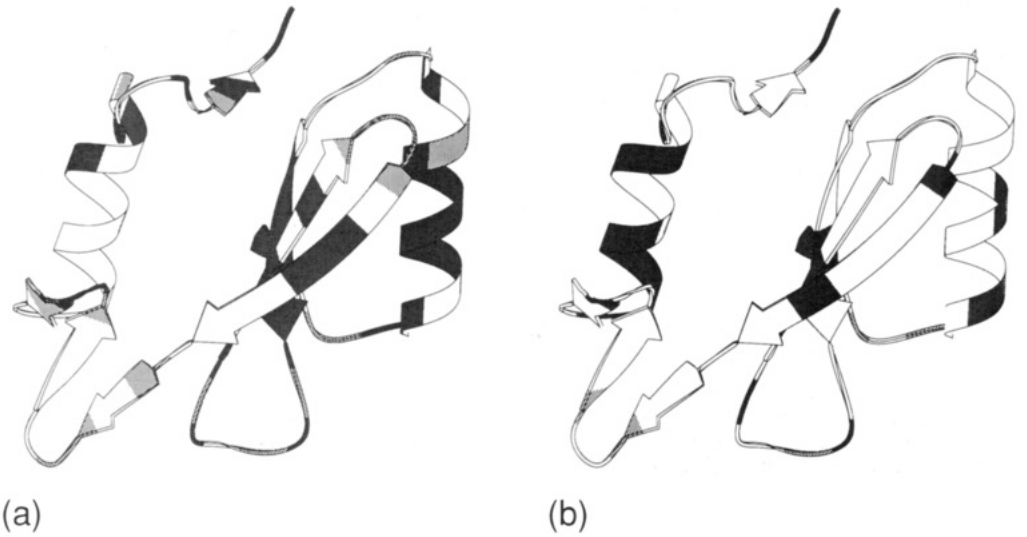

FIGURE 9: Schematic representations of the spatial distributions of residues requiring an R_{ex} term or two-time-scale spectral density functions to fit the measured relaxation data. Residues which required an R_{ex} term are highlighted in dark grey, and residues which required the two-time-scale spectral density function are shown in lighter grey. Residues which required neither of these spectral density functions or for which spectral density functions were not determined are white. The distribution for the uncomplexed form of PLCγ1C is shown in (a); the complexed form is shown in (b). The distributions are imposed on a preliminary structure of PLCγ1C in complex with pY1021 (Pascal et al., 1994). The phosphopeptide is not shown in the diagram. The figure was produced using SETOR (Evans, 1993).

require R_{ex} terms; in the complexed form, only residues Ala 19 and His 23 require an R_{ex} term. In contrast, helix αB shows the opposite trend, with residues Ser 76–Leu 80 all requiring R_{ex} terms in the complexed form of SH2 and not in the peptide-free form. The decreased number of R_{ex} terms required for helix αA upon binding may be due to the fact that N-terminal residue Arg 18 of helix αA is involved in the phosphotyrosine-binding site. The requirement for R_{ex} terms in helix αB in the peptide-complexed form might result not from motion of the helix itself but from a modulation in chemical environment resulting from interactions with the C-terminal residues of the peptide which have been observed to be disordered in both the Lck and Src SH2 structures. Previously, we described how the BG loop in the uncomplexed SH2 domain requires a large number of R_{ex} terms, suggesting that it may be exhibiting motion on a microsecond-to-millisecond-time scale. Unfortunately, data are not available to permit a comparison to determine if this motion is lost upon binding the peptide, since the measured relaxation data for residues Lys 94 and Arg 96 of the complexed form could not be fit by any of the spectral density functions.

A recently reported study of the backbone dynamics of an antibody V_L domain (Constantine et al., 1993) noted that many of the residues which required an R_{ex} term were in close proximity to aromatic side chains. It was postulated that the requirement for an R_{ex} term may be due in part to motion of the nearby rings. Examination of the preliminary structure of the PLCγ1 SH2 domain in light of this observation reveals that a similar hypothesis may also explain some of the R_{ex} requirements that we have observed. In particular, two aromatic residues, Tyr 83 and Tyr 84 in helix αB, appear to be positioned between the helix and the bound peptide. It is of interest to note that cross-peaks correlating the Cβ and Hδ chemical shifts for Tyr 83 and Tyr 84 were conspicuously absent in spectra recorded on the complex using a pulse sequence that we have recently developed to assign aromatic side chains (Yamazaki et al., 1993), suggesting chemical exchange broadening of these resonances. Such motions of the aromatics could, of course, give rise to a broadening of the ^{15}N resonances of helix αB in the complex.

The reduced number of residues requiring the two-time-scale spectral density function in the peptide-complexed form of SH2 suggests that the extent of motion on a 100 ps to $\sim$1 ns time scale is also reduced in the complex. This observation, coupled with the lower number of residues requiring an R_{ex} term in the complex and the approximately equal average S^2 values obtained for uncomplexed and complexed forms of SH2, suggests that it is motions on time scales slower than the picosecond motion characterized by the order parameter S^2 that are lost upon peptide binding. These motions could, of course, also be affected by the monomer–dimer equilibrium in the uncomplexed form.

It is interesting to speculate why significant increases in order parameters are not observed upon peptide binding. Previous studies which have demonstrated increases in order parameters upon ligand binding have shown the effect to be localized to regions close to the binding site. In studies of both calbindin (Kördel et al., 1992; Akke et al., 1993) and staphylococcal nuclease (Nicholson et al., 1992), the ligands were relatively small and binding was achieved through a small number of well-defined interactions. In contrast, the ligand we have considered is much larger, and the binding site is not localized to a single region of the protein. X-ray crystallographic studies of the Src SH2–peptide complex identified 14 key functional residues in the binding site of the protein (Waksman et al., 1993). Similar studies of the Lck SH2–peptide complex identified 17 residues which form the recognition site for the peptide (Eck et al., 1993). Although a single peptide-binding conformation was seen in both of the X-ray crystallographic studies, the size of the binding region and the large number of residues involved in the interaction suggest the possibility that the peptide may exist in multiple conformations when bound. For example, the large positive charge density in the phosphotyrosine-binding pocket and the negative charge density of the π-electron cloud of the tyrosine ring and the phosphate may permit the possibility of multiple binding configurations from nonspecific charge–charge interactions between the phosphotyrosine and the protein. Consistent with this is the large off-rate measured for the peptide in the complex (Felder et al., 1993; Panayotou et al., 1993), suggesting that there may be multiple bound peptide configurations rather than a single preferred one. Indeed, it has been postulated that retention of conformational dynamics

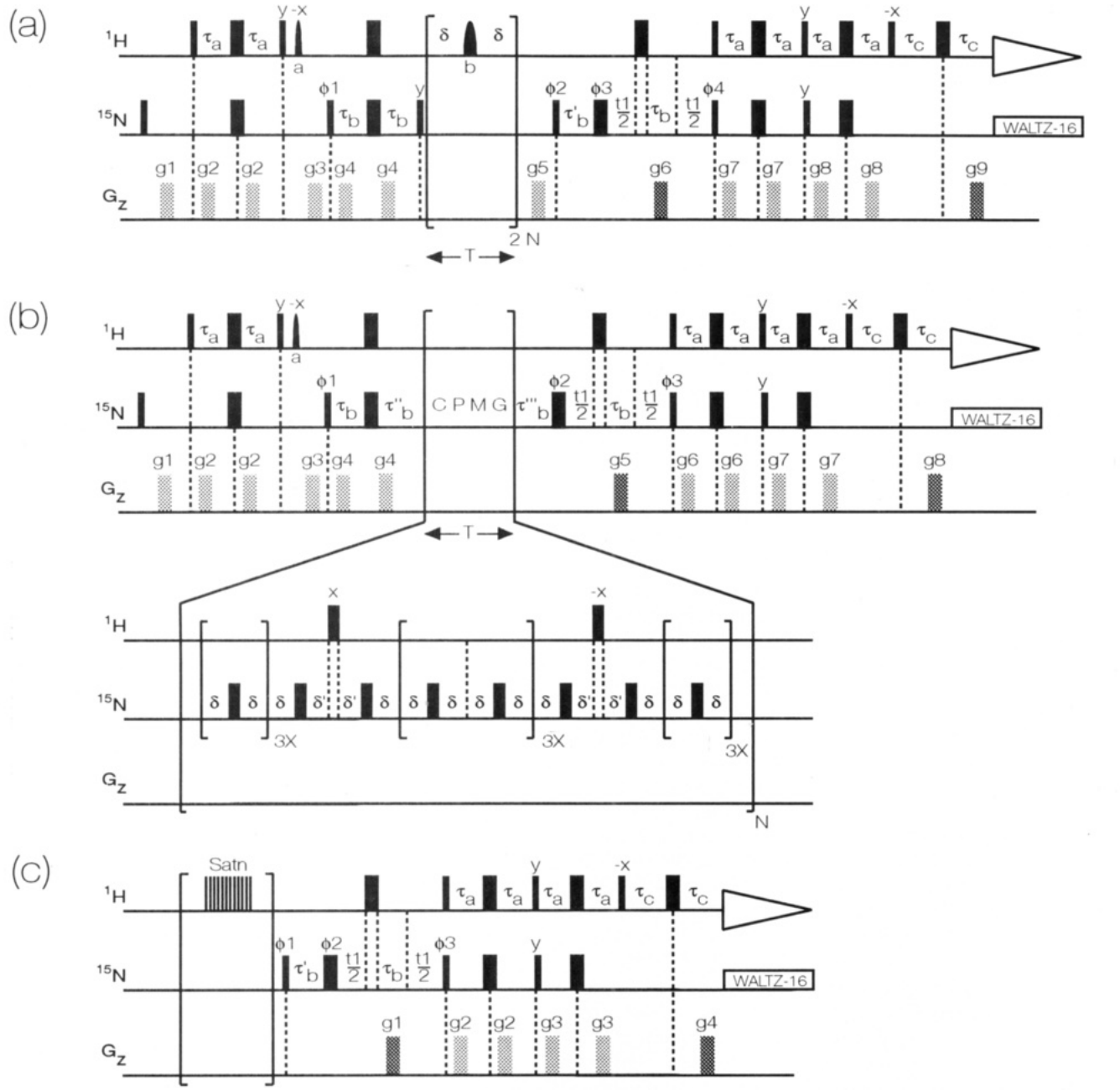

FIGURE 10: Pulse sequences for the measurement of (a) ^{15}N T_1, (b) ^{15}N T_2, and (c) ^1H–^{15}N NOE values with minimal water saturation. In all sequences, narrow and wide pulses indicate 90° and 180° pulses, respectively, darker gradient pulses indicate those used for coherence transfer selection, and, unless indicated otherwise, all pulses are applied along the x-axis. In all experiments, the value of τ_a was set to 2.25 ms ($<1/(4J_{NH})$), τ_b was set to 2.75 ms ($1/(4J_{NH})$), and τ_c was set to 0.5 ms. The delays τ'_b and τ''_b are as defined in the legend to Figure 3. The delay τ'''_b in sequence b is set according to the relation: $\tau'''_b = \tau_b + 2\text{pw} + (2/\pi)\text{pwn}$, where pw and pwn are ^1H and ^{15}N 90° pulse widths, respectively. All pulse widths employed are indicated in the legend to Figure 3. The shaped ^1H 90° pulse at point a in each of the T_1 and T_2 sequences is applied as a 2-ms SEDUCE-1 pulse (~270-Hz field at peak height) (McCoy & Mueller, 1992) or as a 2-ms rectangular pulse (125-Hz field). This pulse is applied with the carrier on the water resonance. The ^1H 180° pulse at point b in the ^{15}N T_1 sequence is a 550-μs cosine-modulated rectangular pulse (Smallcombe, 1993) with excitation maxima positioned 2 kHz from the carrier (on water). This ensures that water magnetization is minimally perturbed by the application of ^1H pulses during the T delay. The phase cycling used for the T_1 experiment was $\phi1 = x, -x$; $\phi2 = y$; $\phi3 = 2(x), 2(y), 2(-x), 2(-y)$; $\phi4 = x$; and receiver was $x, -x, -x, x$. During the period T in the T_1 pulse sequence, an even number of selective pulses were applied. Delay δ was set to 2.5 ms. For each increment of t_1, two FIDS were collected with the phase of $\phi4$ and the amplitude of g6 inverted in the second FID. For each increment of t_1, the phases of $\phi2$ and the receiver are incremented by 180°. Gradient levels used in the T_1 experiment were as follows: g1 = 1 ms, 5 Gcm^{-1}; g2 = 0.5 ms, 4 Gcm^{-1}; g3 = 1 ms, 10 Gcm^{-1}; g4 = 0.5 ms, 8 Gcm^{-1}; g5 = 1 ms, 5 Gcm^{-1}; g6 = 1.25 ms, 30 Gcm^{-1}; g7 = 0.5 ms, 4 Gcm^{-1}; g8 = 0.5 ms, 4 Gcm^{-1}; and g9 = 0.125 ms, 27.8 Gcm^{-1}. The phase cycling used for the T_2 pulse sequence was $\phi1 = x, -x$; $\phi2 = 2(x), 2(y), 2(-x), 2(-y)$; $\phi3 = x$; and receiver was $x, -x, -x, x$. The delay δ in the CPMG sequence was set to 0.45 ms; the delay δ' was set according to the relation: $\delta' = \delta - \text{pw}$, where pw is the ^1H 90° pulse width. For each increment of t_1, two FIDS were collected with the phase of $\phi3$ and the amplitude of g5 inverted in the second FID. For each increment of t_1, the phases of $\phi1$ and the receiver are incremented by 180°. Gradient levels used in the T_2 experiment were as follows: g1 = 1 ms, 5 Gcm^{-1}; g2 = 0.5 ms, 4 Gcm^{-1}; g3 = 1 ms, 10 Gcm^{-1}; g4 = 0.5 ms, 8 Gcm^{-1}; g5 = 1.25 ms, 30 Gcm^{-1}; g6 = 0.5 ms, 4 Gcm^{-1}; g7 = 0.5 ms, 4 Gcm^{-1}; and g8 = 0.125 ms, 27.8 Gcm^{-1}. The phase cycling used for the NOE experiment was $\phi1 = y$; $\phi2 = x, y, -x, -y$; $\phi3 = x$; and receiver was $x, -x$. For each increment of t_1, two FIDS were collected with the phase of $\phi3$ and the amplitude of g1 inverted in the second FID. For each increment of t_1, the phases of $\phi1$ and the receiver are incremented by 180°. Gradient levels used in the NOE experiment were as follows: g1 = 1.25 ms, 30 Gcm^{-1}; g2 = 0.5 ms, 4 Gcm^{-1}; g3 = 0.5 ms, 4 Gcm^{-1}; and g4 = 0.125 ms, 27.8 Gcm^{-1}.

can play an entropically favorable role in protein–protein interactions (Lumry & Gregory, 1989).

It is also interesting to consider our results in light of recent X-ray crystallographic studies of the human class I MHC molecule in complex with five viral peptides between 9 and 10 residues in length (Madden et al., 1993). This study revealed that the five bound peptides adopted similar conformations at their N- and C-termini where there are a number of well-defined, tight binding interactions. In contrast, the central residues of the bound peptide were seen to adopt a variety of more flexible conformations in the binding site. The binding site of the HLA-A2 MHC molecule itself showed only small levels of structural variability between the different complexes. While there are differences between the binding sites of SH2 domains and that of the HLA-A2 molecule, most notably that the binding site of the SH2 domain is smaller and that the cognate peptide is not engulfed to the same extent, it is interesting to speculate whether similar configurational freedom may also exist in the phosphopeptide–SH2 complex. The fact that single SH2 domains are able to bind phosphotyrosine residues in a variety of sequence contexts suggests that a similar mechanism for accommodation of sequence differences may exist in SH2 domains.

In contrast to the study of MHC-bound peptides, the comparative study of Src SH2 (Waksman et al., 1993) showed slight but significant structural differences for two of the four independent molecules of the uncomplexed form when compared to the peptide-bound form. The most notable structural changes occurred in the BC and EF loops. The other two uncomplexed molecules closely resembled the complexed form of the domain. While the variation in structures seen in the uncomplexed molecules is suggestive of greater conformational freedom, it is interesting to note that the crystallographic B-factors of the backbone α-carbons show, on average, only a 12% reduction in the BC loop upon binding and that the EF loop exhibits 12% higher B-factors in the complexed form. This suggests that there is not a large change in the conformational freedom of these regions upon peptide binding, consistent with the observations reported here.

The observed loss of picosecond-time-scale motion upon ion binding in calbindin is thought to be related to restriction of motion of an initially disordered loop. In the case of the SH2 domain, we do not see evidence for high levels of disorder throughout the putative binding site of the uncomplexed form, an exception to this observation being the BC loop. The order parameters observed were similar to those seen in other proteins, and because a large fraction of the SH2 domain is involved in peptide binding, it would have been surprising to have observed markedly lower order parameters throughout the binding site of the domain in the uncomplexed form.

In conclusion, the results of the present study do not support the contention that picosecond-time-scale motion is restricted upon peptide binding. This is somewhat suprising in light of other ligand-binding studies. However, we propose that the binding of a large ligand, such as the peptide, is likely to have different effects on the backbone dynamics than those seen for smaller ligands. The large peptide–protein interface offers the possibility of many different interactions between the peptide and the protein, and it is possible that the peptide is not bound in a single conformation. This possibility is supported, on the one hand, by the observation that peptide–protein interactions were not identical in all three molecules in the asymmetric unit of Src (Waksman et al., 1993) and, on the other hand, by NMR results which show that cross-peaks of many of the protein residues that line the binding site are broadened or display multiple peaks in the spectra of the SH2 complex (Yamazaki et al., 1993). The results we have presented here characterize the effect of protein–protein interactions upon protein backbone dynamics and provide insights which suggest that a simple relationship between peptide binding and large-scale restriction of picosecond-time-scale dynamics in the binding site does not hold.

ACKNOWLEDGMENT

We thank Professor John Kuriyan, Rockefeller University, for making available the coordinates of the uncomplexed and complexed Src SH2 structures and Mr. Les Hicks, Department of Biochemistry, University of Alberta, for valuable technical assistance.

APPENDIX

A recent paper by Grzesiek and Bax (1993) as well as work in our laboratory (Kay et al., 1994) has indicated the importance of minimizing water saturation in experiments recorded on molecules dissolved in H_2O. This can be readily achieved in the enhanced sensitivity pulse schemes described in Figure 3 by (i) inserting a single water-selective pulse at positions marked a in the pulse sequences indicated in Figure 10; (ii) making use of ^1H 180° pulses that do not excite the water resonance during the T delay used to measure ^{15}N T_1 relaxation times; and (iii) paying close attention to the phases of the ^1H pulses. The pulse sequences in Figure 10 minimize water saturation, maintain a high degree of artifact suppression, and offer enhanced sensitivity (Kay et al., 1992a).

SUPPLEMENTARY MATERIAL AVAILABLE

Table containing T_1, T_2, and NOE values for both the uncomplexed and complexed forms of PLCγ1C SH2 (4 pages). Ordering information is given on any current masthead page.

REFERENCES

Abragam, A. (1961) *Principles of Nuclear Magnetism*, Clarendon Press, Oxford.

Akke, M., Skelton, N. J., Kördel, J., Palmer, A. G., III, & Chazin, W. J. (1993) *Biochemistry 32*, 9832.

Anderson, D., Koch, C. A., Grey, L., Ellis, C., Moran, M. F., & Pawson, T. (1990) *Science 250*, 979.

Barbato, G., Ikura, M., Kay, L. E., Pastor, R. W., & Bax, A. (1992) *Biochemistry 31*, 5269.

Bax, A., & Pochapsky, S. (1992) *J. Magn. Reson. 99*, 638.

Booker, G. W., Breeze, A. L., Downing, A. K., Panayotou, G., Gout, I., Waterfield, M. D., & Campbell, I. D. (1992) *Nature 358*, 684.

Boyd, J., Hommel, U., & Campbell, I. D. (1990) *Chem. Phys. Lett. 175*, 477.

Cantor, C. R., & Schimmel, P. R. (1980) *Biophysical Chemistry*, p 563, Freeman, San Francisco.

Carr, H. Y., & Purcell, E. M. (1954) *Phys. Rev. 4*, 630.

Cavanagh, J., Palmer, A. G., III, Wright, P. E., & Rance, M. (1991) *J. Magn. Reson. 91*, 429.

Chervenka, C. H. (1969) *A Manual for the Analytical Ultracentrifuge*, Spinco Division of Beckman Instruments Inc., Palo Alto, CA.

Clore, G. M., Driscoll, P. C., Wingfield, P. T., & Gronenborn, A. M. (1990a) *Biochemistry 29*, 7387.

Clore, G. M., Szabo, A., Bax, A., Kay, L. E., Driscoll, P. C., & Gronenborn, A. M. (1990b) *J. Am. Chem. Soc. 112*, 4989.

Constantine, K. L., Friedrichs, M. S., Goldfarb, V., Jeffrey, P. D., Sheriff, S., & Mueller, L. (1993) *Proteins: Struct., Funct., Genet. 15*, 290.

Eck, M. J., Shoelson, S. E., & Harrison, S. C. (1993) *Nature 362*, 87.

Evans, S. V. (1993) *J. Mol. Graphics 11*, 134.
Felder, S., Zhou, M., Hu, P., Urena, J., Ullrich, A., Chaudhuri, M., White, M., Shoelson, S. E., & Schlessinger, J. (1993) *Mol. Cell. Biol. 13*, 1449.
Grzesiek, S., & Bax, A. (1993) *J. Am. Chem. Soc. 115*, 12593.
Hiyama, Y., Niu, C., Silverton, J. V., Bavoso, A., & Torchia, D. A. (1988) *J. Am. Chem. Soc. 110*, 2378.
Kamath, U., & Shriver, J. W. (1989) *J. Biol. Chem. 264*, 5586.
Kay, L. E., Torchia, D. A., & Bax, A. (1989) *Biochemistry 28*, 8972.
Kay, L. E., Keifer, P., & Saarinen, T. (1992a) *J. Am. Chem. Soc. 114*, 10663.
Kay, L. E., Nicholson, L. K., Delaglio, F., Bax, A., & Torchia, D. A. (1992b) *J. Magn. Reson. 97*, 359.
Kay, L. E., Xu, G. Y., & Yamazaki, T. (1994) *J. Magn. Reson.* (in press).
Kördel, J., Skelton, N. J., Akke, M., Palmer, A. G., III, & Chazin, W. J. (1992) *Biochemistry 31*, 4856.
Kraulis, P. (1991) *J. Appl. Crystallogr. 24*, 946.
Larose, L., Gish, G., Shoelson, S. E., & Pawson, T. (1993) *Oncogene 8*, 2493.
Lipari, G., & Szabo, A. (1982a) *J. Am. Chem. Soc. 104*, 4546.
Lipari, G., & Szabo, A. (1982a) *J. Am. Chem. Soc. 104*, 4559.
Lumry, R., & Gregory, R. B. (1989) *J. Mol. Liquids 42*, 113.
Madden, D. R., Garboczi, D. N., & Wiley, D. C. (1993) *Cell 75*, 693.
Marion, D., Ikura, M., & Bax, A. (1989) *J. Magn. Reson. 84*, 425.
Markley, J. L., Horsley, W. J., & Klein, M. P. (1971) *J. Chem. Phys. 55*, 3604.
McCoy, M., & Mueller, L. (1992) *J. Am. Chem. Soc. 114*, 2108.
Meiboom, S., & Gill, D. (1958) *Rev. Sci. Instrum. 29*, 688.
Messerlie, B. A., Wider, W., Otting, G., Weber, C., & Wutrich, K. (1989) *J. Magn. Reson. 85*, 608.
Muhandiram, D. R., & Kay, L. E. (1994) *J. Magn. Reson.* (in press).
Nicholson, L. K., Kay, L. E., Baldisseri, D. M., Arango, J., Young, P. E., Bax, A., & Torchia, D. A. (1992) *Biochemistry 31*, 5253.
Overduin, M., Rios, C. B., Mayer, B. J., Baltimore, D., & Cowburn, D. (1992) *Cell 70*, 697.
Palmer, A. G., III, Rance, M., & Wright, P. E. (1991) *J. Am. Chem. Soc. 113*, 4371.
Palmer, A. G., III, Skelton, N. J., Chazin, W. J., Wright, P. E., & Rance, M. (1992) *Mol. Phys. 75*, 699.
Panayotou, G., Gish, G., End, P., Truong, O., Gout, I., Dhand, R., Fry, M. J., Hiles, I., Pawson, T., & Waterfield, M. D. (1993) *Mol. Cell. Biol. 13*, 3567.
Pascal, S. M., Singer, A. U., Gish, G., Yamazaki, T., Shoelson, S. E., Pawson, T., Kay, L. E., & Forman-Kay, J. D. (1994) *Cell* (in press).
Pawson, T., & Schlessinger, J. (1993) *Curr. Biol. 3*, 434.
Piccione, E., Case, R. D., Domchek, S. M., Hu, P., Chaudhuri, M., Backer, M., Schlessinger, J., & Shoelson, S. E. (1993) *Biochemistry 32*, 3197.
Press, W. H., Flannery, B. P., Teukolsky, S. A., & Vetterling, W. T. (1986) *Numerical Recipes*, Cambridge University Press, Cambridge.
Schneider, D. M., Dellwo, M. J., & Wand, A. J. (1992) *Biochemistry 31*, 3645.
Shaka, A. J., Keeler, J., Frenkiel, T., & Freeman, R. (1983) *J. Magn. Reson. 52*, 335.
Sklenar, V., Torchia, D. A., & Bax, A. (1987) *J. Magn. Reson. 73*, 375.
Smallcombe, S. (1993) *J. Am. Chem. Soc. 115*, 44776.
Songyang, Z., Shoelson, S. E., Chaudhuri, M., Gish, G., Pawson, T., Haser, W. G., King, F., Roberts, T., Ratnofsky, S., Lechleider, R. J., Neel, B. G., Birge, R. B., Fajardo, J. E., Chou, M. M., Hanafusa, H., Schaffhausen, B., & Cantley, L. C. (1993) *Cell 72*, 767.
States, D. I., Haberkorn, R. A., & Ruben, D. J. (1982) *J. Magn. Reson. 48*, 286.
Stone, M. J., Fairbrother, W. J., Palmer, A. G., III, Reizer, J., Saier, M. H., Jr., & Wright, P. E. (1992) *Biochemistry 31*, 4394.
Stone, M. J., Chandrasekhar, K., Holmgren, A., Wright, P. E., & Dyson, H. J. (1993) *Biochemistry 32*, 426.
Valius, M., Bazenet, C., & Kazlauskas, A. (1993) *Mol. Cell. Biol. 13*, 133.
Venable, R. M., & Pastor, R. W. (1988) *Biopolymers 27*, 1001.
Waksman, G., Kominos, D., Robertson, S. C., Pant, N., Baltimore, D., Birge, R. B., Cowburn, D., Hanafusa, H., Mayer, B. J., Overduin, M., Resh, M. D., Rios, C. B., Silverman, L., & Kuriyan, J. (1992) *Nature 358*, 646.
Waksman, G., Shoelson, S. E., Pant, N., Cowburn, D., & Kuriyan, J. (1993) *Cell 72*, 779.
Wyatt, P. J. (1993) *Anal. Chim. Acta 272*, 1.
Yamazaki, T., Forman-Kay, J. D., & Kay, L. E. (1993) *J. Am. Chem. Soc. 115*, 11054.